

DIGITAL ROCK PHYSICS FOR MULTISCALE CHARACTERIZATION OF
HETEROGENEOUS PETROLEUM GEOMATERIALS

by

Jan Goral

A thesis submitted to the faculty of
The University of Utah
in partial fulfillment of the requirements for the degree of

Master of Science

Department of Mining Engineering

The University of Utah

August 2017

Copyright © Jan Goral 2017

All Rights Reserved

ABSTRACT

The ever-growing energy demand and recent discoveries of vast unconventional oil and gas reservoirs have brought significant attention to shale oil and gas resources as potential game-changers for the petroleum industry and energy markets worldwide. Although shale reservoirs are large in scale and offer the potential for long-lived production, extremely low matrix porosity and permeability, as well as complex heterogeneity, pose major challenges in obtaining economically viable oil and gas. A lack of predictive understanding of microstructure-based heterogeneity in shale rock limits the effectiveness of currently used exploration and production technologies. Hence, addressing the challenges of shale oil and gas exploration and production technology requires an in-depth understanding of microstructural features that control the oil and gas subsurface transport phenomena.

A new holistic approach for characterization of multiscale structural heterogeneity in shale, presented in this thesis, couples micro- and nano-X-ray microscopy (micro- and nano-XRM) with focused ion beam scanning electron microscopy (FIB-SEM). This integrated approach provides a unique opportunity to characterize in great detail the complex three-dimensional (3D) microstructure of shale rock over multiple length scales, from the centimeter length scale to the single nanometers. To explore the practical significance and reach of this newly developed analytical framework, samples from the Woodford Shale and the Marcellus Shale were imaged several times with non-destructive

XRM at successively higher resolutions, and then finally imaged with the high-resolution by destructive FIB-SEM serial-sectioning. Subsequently, in order to quantify the evolution of porosity associated with both organic and nonorganic (mineral) matter, the organic- and nonorganic-matter pore networks within both samples were extracted using the FIB-SEM models.

The digital rock physics (DRP) 3D image-based characterization revealed the Woodford Shale and the Marcellus Shale samples to be primarily composed of varying amounts of organic and mineral matter. The findings also indicate complex pore systems, both within organic and nonorganic matrices. The pore network modeling (PNM) analysis suggested that pores and microfractures located at the interface between organic and mineral matter were the most abundant pore types in analyzed shale rock samples, and have the potential for better connectivity. Finally, representative pore/fracture networks, for continuum and non-continuum fluid flow studies, were separated and transformed into finite element models for future works.

To My Family

TABLE OF CONTENTS

ABSTRACT	iii
LIST OF TABLES	viii
LIST OF FIGURES	ix
ACKNOWLEDGMENTS	xii
Chapters	
1. INTRODUCTION	1
2. LITERATURE REVIEW	3
2.1 Conventional and Unconventional Oil and Gas	3
2.2 Reservoir Quality and Completion Quality	5
2.3 Pore-, Core-, and Reservoir-Scale Characterization	6
2.4 Organic vs. Nonorganic (Mineral) Matter	7
2.5 Heterogeneous Shale Reservoir Pore Systems	9
2.6 Digital Rock Physics (DRP)	10
2.6.1 X-ray Microscopy (XRM)	11
2.6.2 Focused Ion Beam Scanning Electron Microscopy (FIB-SEM).....	13
2.6.3 XRM/FIB-SEM Correlative Microscopy	14
3. RESEARCH STATEMENT	21
4. METHODS	23
4.1 Sample Preparation for SEM and/or FIB-SEM	24
4.2 XRM/FIB-SEM Correlative Microscopy for the Woodford Shale and the Marcellus Shale.....	25
4.2.1 Case Study I: The Woodford Shale	25
4.2.2 Case Study II: The Marcellus Shale.....	28
5. RESULTS AND DISCUSSION	36
5.1 Case Study I: The Woodford Shale	36
5.1.1 Pore Network Modeling (PNM) in the Woodford Shale	39
5.2 Case Study II: The Marcellus Shale.....	42
5.2.1 Pore Network Modeling (PNM) in the Marcellus Shale	43

5.3 Woodford Shale vs. Marcellus Shale Reservoir Pore System	44
5.4 Image to Simulation Workflow for Continuum and Non-Continuum Transport Phenomena in Heterogeneous Shale Reservoir Pore Systems	45
5.4.1 A Workflow for Continuum Fluid Flow in Heterogeneous Shale Reservoir Pore Systems	46
5.4.2 A workflow for Non-Continuum Fluid Flow in Heterogeneous Shale Reservoir Pore Systems	47
6. CONCLUSIONS.....	68
REFERENCES	70

LIST OF TABLES

Tables

4.1. Woodford Shale and Marcellus Shale samples' location information.....	30
5.1. Phase separation and quantification of the focused ion beam scanning electron microscopy (FIB-SEM) model of the Woodford Shale of the region I.	48
5.2. Phase separation and quantification of the focused ion beam scanning electron microscopy (FIB-SEM) model of the Woodford Shale of the region II.	49
5.3. Phase separation and quantification of the focused ion beam scanning electron microscopy (FIB-SEM) model of the Marcellus Shale.	50
5.4. Tetrahedron volume mesh of the pore network, organic matter, and nonorganic matter.	51

LIST OF FIGURES

Figures

2.1. Shale oil and gas plays in the United States.	15
2.2. Shale gas production from selected plays in the United States through the years 2002-2016.	16
2.3. Tight oil production from selected plays in the United States through the years 2002-2016.	17
2.4. Dry natural gas production by source in the United States through the years 1990-2040.	18
2.5. Shale rock matrix composition classification.	19
2.6. Focused ion beam (FIB) scanning electron microscopy (SEM) serial-sectioning. ...	20
4.1. Sample preparation with argon ion beam milling system.	30
4.2. Correlative micro-X-ray microscopy (micro-XRM), nano-X-ray microscopy (nano-XRM), and focused ion beam scanning electron microscopy (FIB-SEM) workflow for the Woodford Shale.	31
4.3. Schematic diagram illustrating the principles of operation of micro-X-ray microscope (micro-XRM).	32
4.4. Schematic diagram illustrating the principles of operation of nano-X-ray microscope (nano-XRM).	33
4.5. Sample preparation with laser ablation system.	33
4.6. Correlative (micro and nano) X-ray microscopy (XRM) workflow for the Woodford Shale.	34
4.7. Schematic diagram illustrating the principle of operation of focused ion beam scanning electron microscope (FIB-SEM).	34
4.8. Correlative nano-X-ray microscope (nano-XRM) and focused ion beam scanning electron microscopy (FIB-SEM) workflow for the Marcellus Shale.	35

5.1. Scanning electron microscopy (SEM) image of the Woodford Shale. 52

5.2. Automated mineralogy and petrography (A) 10 um resolution and (B) 2 um resolution mosaic image of the Woodford Shale. 52

5.3. (A) 25-mm diameter micro-XRM (25 um resolution), (B) 2.5-mm diameter micro-XRM (2.5 um resolution), and (C) 65-um diameter nano-XRM (150 nm resolution) models of the Woodford Shale. 53

5.4. From image processing and segmentation, through model reconstruction and visualization, to pore network modeling workflow. 53

5.5. Focused ion beam scanning electron microscopy (FIB-SEM) model of (A) organic matter, (B) nonorganic matter, and (C) pore network within the Woodford Shale. 54

5.6. Pore types within 5 μm³ shale rock matrix. 55

5.7. Pore network separation into (A) organic-matter-hosted pores and (B) nonorganic-matter-hosted pores within the Woodford Shale. 56

5.8. Pore size distribution of the organic-matter-hosted pores within the Woodford Shale. 57

5.9. Pore size distribution of the nonorganic-matter-hosted pores within the Woodford Shale. 58

5.10. Connected pore network model of (A) organic-matter-hosted and (B) nonorganic-matter-hosted pores within the Woodford Shale. 59

5.11. Focused ion beam scanning electron microscopy (FIB-SEM) model of the Woodford Shale divided into (A) region I and (B) region II. 60

5.12. Pore network separation into (A) organic-matter-related and (B) nonorganic-matter-related pore network within the Woodford Shale in the region I. 61

5.13. Pore network separation into (A) organic-matter-related and (B) nonorganic-matter-related pore network within the Woodford Shale in the region II. 61

5.14. Focused ion beam scanning electron microscopy (FIB-SEM) model of (A) organic matter, (B) nonorganic matter, (C) total pore network, and (D) connected pore network within the Marcellus Shale. 62

5.15. Pore network separation into (A) organic-matter-hosted pores and (B) nonorganic-matter-hosted pores within the Marcellus Shale. 63

5.16. Pore size distribution of the organic-matter-hosted pores within the Marcellus Shale. 64

5.17. Pore size distribution of the nonorganic-matter-hosted pores within the Marcellus Shale.....	64
5.18. Connected pore network model of (A) organic-matter-hosted and (B) nonorganic-matter-hosted pores within the Marcellus Shale.	65
5.19. Pore network separation into (A) organic-matter-related pores and (B) nonorganic-matter-related pores within the Marcellus Shale.	66
5.20. Tetrahedron volume mesh of the pore/fracture network.....	67
5.21. Three-phase (pore network, organic matter, and nonorganic matter) 1 μm x 1 μm x 2 μm region of interest (ROI) of the FIB-SEM model of the Woodford Shale.....	67

ACKNOWLEDGMENTS

The author would like to express his sincere gratitude to his supervisor, Dr. Ilija Miskovic, for a constant supply of encouragement, guidance, and advice. Additionally, the author wishes to gratefully acknowledge the help and support of his committee members, Dr. Michael Nelson and Dr. Raymond Levey.

The thesis programme would not have been possible without constant advice and cooperation from professors, graduate students, and academic staff of the College of Mines and Earth Sciences at the University of Utah.

Special credit is due to Dr. Jan Hupka for his help and support.

Special gratitude is due to the Idaho National Laboratory (INL), particularly Dr. Earl Mattson and Dr. Hai Huang for their precious guidance and suggestions during my internship.

Further thanks are due to the Carl Zeiss Microscopy, including Jack Kasahara and Jeff Gelb, for supporting much of this work.

Further gratitude is due to National Energy Technology Laboratory (NETL) and U.S. Geological Survey (USGS) Core Research Center for providing access to core rock materials.

Finally, my sincere thanks to my family, for their encouragement, support, and patience.

CHAPTER 1

INTRODUCTION

Owing to depleting conventional hydrocarbon reserves, unconventional oil and gas resources have grown in importance as global energy demand has increased. Shale oil and gas is expected to be a major unconventional energy source for future generations in all parts of the world. Despite the discovery of a large number of proven shale oil and gas reserves across the world, the oil and gas industry is facing numerous technical and environmental challenges that are limiting feasibility of the shale oil and gas production. The main challenge is that only a small fraction can be recovered using the latest technology, due to the lack of basic science needed to understand the technology and to guide additional advances. Concepts and theories developed for conventional oil and gas reservoirs cannot be readily transferred and applied to shale oil and gas systems. Today, there is still wide gap in the knowledge and understanding of the relevant fundamental physics that ultimately control the transport phenomena in the subsurface. Filling these gaps could facilitate the development and deployment of effective technology in important energy and environmental applications.

In this study, in Chapter 2, I will start with a brief literature review on reservoir quality and completion quality in the context of unconventional oil and gas exploration and production. Later in this thesis, in Chapter 4, I will introduce digital rock physics

technology, as an emerging multiscale characterization method for heterogeneous petroleum geomaterials, followed by the experimental procedure (in Chapter 5) applied to study Woodford Shale and Marcellus Shale rock samples. In Chapter 6, I will present pore network modeling results supported with a discussion. Finally, I will end with conclusions in Chapter 7.

CHAPTER 2

LITERATURE REVIEW

Before the recent downturn in the upstream petroleum industry sector, development of unconventional oil and gas resources had a terrific run and had a profound impact on hydrocarbons supply, especially in the United States and Canada.

“A downturn gives us some time to step back, review what has been done, and think about possible improvements and innovations” (Ma and Holditch 2016).

2.1 Conventional and Unconventional Oil and Gas

The number of conventional oil and gas discoveries had been growing for several decades until the mid-1980s, when it started to decrease along with the decreasing amount of reserves found each year (Hyne 2012). Unconventional oil and gas resources, such as heavy oil sands, shale oil and gas, tight gas sandstones, coalbed methane, and gas hydrates, will become more important with time to replace conventional oil and gas.

Conventional oil and gas resources usually accumulate in favorable structural or stratigraphic traps in which the formation is porous and permeable (above 0.1 mD), but also sealed by an impermeable layer that prevents hydrocarbons from escaping.

Conventional reservoirs are those that have good reservoir quality and generally can be

economically developed using vertical wellbores and without the use of massive hydraulic fracture stimulation treatment.

On the other hand, unconventional subsurface hydrocarbon resources reside in tight formations, which are of lower reservoir quality and are much more difficult in terms of hydrocarbons extraction. Unconventional reservoirs are often characterized by very low porosity and permeability (below 0.1 mD) and must be developed using a combination of horizontal drilling and multistage hydraulic fracturing to produce hydrocarbons at an acceptable recovery rate (Ambrose et al. 2010 and 2012, Bai 2011, Ding et al. 2012, King 2012). For example, the typical recovery factor for shales is estimated to be about 15 to 35% of the gas in place (Hyne 2012).

One of the tight formations are shales and they are the most abundant sedimentary rock on Earth. Shale formations are combination of source rock, reservoir rock, and a seal, that has generated oil and gas, but not all the hydrocarbons have been expelled from the rock. The oil and gas are contained in pore spaces, natural fractures, and adsorbed onto organic matter. There is a very large number of shale plays in the United States, Canada, and throughout the world. Some of the most prolific oil and gas producing shale formations in the U.S. include Barnett Shale in north-central Texas, Fayetteville Shale in northern Arkansas, Haynesville Shale in eastern Texas and north Louisiana, Woodford Shale in Oklahoma, Eagle Ford in southern Texas, and Marcellus Shale and Utica Shale in northern Appalachia (Figure 2.1).

Figure 2.2 and Figure 2.3 depict total shale gas and tight oil production (from different shale formations) in the United States from 2012 to 2016. Estimates by the U.S. Energy Information Administration (EIA) suggest that the United States has

approximately 610 Tcf of technically recoverable shale natural gas resources, and 59 billion barrels of technically recoverable tight oil resources (EIA 2014). Note that the term “tight oil” refers to all resources, reserves, and production associated with low-permeability formations that produce oil, including those associated with shale formations.

According to EIA, production from shale gas and tight oil plays is the largest contributor to U.S. oil and gas, and is expected to increase from 50% in 2015 to 69% in 2040, growing by more than 15 Tcf, from 13.6 Tcf in 2015 to 29 Tcf in 2040, as depicted in Figure 2.4 (EIA 2014).

2.2 Reservoir Quality and Completion Quality

There is no unique geological, geophysiochemical, or geomechanical parameter that can determine oil or gas production, but two categories of variables are important: reservoir quality (RQ) and completion quality (CQ).

RQ describes oil or gas potential, the amount of oil and gas in place, and oil and gas deliverability of the rock formation. The important variables in reservoir quality include lithology, thermal maturity, organic and nonorganic (mineral) content, total organic carbon (TOC), total and connected (effective) porosity, absolute/effective/relative permeability, fluid saturations, and formation pressure (Passey et al. 2010).

CQ, on the other hand, describes stimulation potential or the ability to create and maintain natural and induced fracture surface area. Completion quality is highly dependent on geomechanical properties and mineralogical composition of the rock formation, including in-situ stress regime and rock fracturability (Nadimi et al. 2016,

Waters et al. 2011, Weng et al. 2015). For example, one principle in selecting a zone for hydraulic fracturing based on completion quality is to target the rocks that have a high Young's modulus and a low Poisson ratio (Ma 2016). A brittle rock responds to hydraulic fracturing better than an elastic rock. Shales with some silica or calcium carbonate are more brittle than shales with more clay minerals (Hyne 2012).

Evaluation of shale oil and gas resources, by judging whether a given shale formation has a sufficient amount of technically recoverable hydrocarbons, requires a multidisciplinary approach (see Chapter 2.3). It must correlate all of the geological, petrophysical, and geomechanical variables in the reservoir and completion quality so that horizontal drilling and hydraulic fracturing (e.g., lateral length, stage count, frac fluid composition, and proppant tonnage) are designed optimally for achieving the best economics.

2.3 Pore-, Core-, and Reservoir-Scale Characterization

Shale oil and gas reservoirs are heterogeneous at many scales – pore-, core-, and reservoir-scale – and are often referred to as statistical plays due to their degree of anisotropy, which presents tremendous challenge for exploration and production (Nadimi 2015). The heterogeneity of gas- and liquid-rich shale reservoirs is manifested as variability in reservoir properties, including geological, geophysicochemical, and geomechanical characteristics. It results from the combination of different physical, chemical, and biogenic processes occurring during, and shortly after, sediment deposition (Aplin and Macquaker 2011). For instance, porosity/permeability (por/permeability) of a shale reservoir is never a constant value, because reservoir por/permeability heterogeneity is very high.

This makes these unconventional reservoirs extremely complex and challenging to assess reservoir or completion quality. Therefore, evaluation and development of shale reservoirs is not a straightforward process and requires a multidisciplinary approach that must integrate geological, petrophysical, and geomechanical variables including: lithology, thermal maturity, organic and mineral content, TOC, pore/fracture network, permeability, fluid saturations, formation pressure, fluid/rock interaction, etc. By integrating all the available information over multiple scales into the workflow, this should enable better characterization of reservoir properties, ranking critical parameters, and optimizing production, managing and reducing the uncertainty and risk in developing unconventional resources.

2.4 Organic vs. Nonorganic (Mineral) Matter

As previously mentioned, shale is the most common sedimentary rock (~ 99%) and is composed of finely-grained organic matter and nonorganic (mineral) matter. Depending on the organic content, the color of shale commonly ranges from black to gray. The darker the shale, the higher the organic content. Black shale is common source rock for oil and gas. A gray shale can be a caprock on a reservoir rock in a petroleum trap. Shales are commonly deposited on river floodplains and on the bottom of lakes or oceans. Depending on the depositional environment, there are two types of organic matter that can be found in shale rocks: land-derived and aquatic-algae-derived. A combination of time, temperature, and pressure converts organic matter into kerogen and then into hydrocarbons over three main stages of maturation: diagenesis, catagenesis, and metagenesis (Pathak et al. 2015a). Converting kerogen into hydrocarbons often causes

increased pressure and porosity within the source rock (see Chapter 2.5). The amount of oil and gas generated is determined by the kerogen type and the heating rate (thermal maturity). There are four types of kerogen found (separately or together) in shale: lacustrine oil prone type I, marine oil and gas prone (depending on the kerogen maturity) type II, terrestrial gas or condensate prone type III, and type IV (with little capacity for hydrocarbons generation) (Pathak et al. 2017a). Kerogen type and its evolution into oil and gas can be illustrated by the Van Krevelen diagram (Pathak et al. 2017b). The type of kerogen present in a shale formation determines source rock quality (the more oil-prone a kerogen, the higher its quality). Examples of oil-bearing organic-rich shales are Bakken, Monterey, and Eagle Ford Shale formations, while the examples of gas-bearing organic-rich shales are Barnett, Fayetteville, and Marcellus Shale formations (Ma 2016). In unconventional reservoirs, similarly to organic matter, mineral matter composition plays an important role in reservoir and completion quality evaluation, as it may govern fluid flow and storage (Heath et al. 2011). In general, shales can be mineralogically described using a ternary diagram with three dominant mineral components: clay, carbonates, and silicates. Figure 2.5 depicts shale rock matrix composition classification. Most well-known productive shale reservoirs are highly siliceous, but a few known shale reservoirs have high calcareous content, like Niobrara or Eagle Ford Shale formations (Ma 2016). However, individual shale reservoirs can vary considerably in mineralogy, due to unconventional reservoir heterogeneity. Therefore, a proper understanding of geological settings of the shale reservoir along with its mineralogical mix is essential.

2.5 Heterogeneous Shale Reservoir Pore Systems

Heterogeneous shale reservoir pore systems have been the focus of many academic institutions and industrial research and development groups (Curtis et al. 2010, Dewers et al. 2012, Goral et al. 2015a, Lonoy 2006, Milliken et al. 2013, Pommer and Milliken 2015). Their studies have shown that both the organic and mineral matter found within shale rock matrix have a variety of pore networks that can be any combination of pore types and (natural or induced) microfractures of different pore sizes, from a few nanometers to several microns in size. Both pores and microfractures form the flow pathways for hydrocarbon migration in shale reservoirs. According to Loucks et al. (2010 and 2012), there are three main categories of pore types in shales classified based on their relationship with grains: organic-matter intragranular pores, mineral-matter intragranular pores, and mineral-matter intergranular pores. Intergranular pores are located between grains and crystals, whereas intragranular pores are found within particles. Organic-matter intragranular pores, also known as intraparticle pores, appear to be related to thermal maturation of organic matter, whereas mineral-matter intraparticle and interparticle pores are strongly affected by mechanical and chemical diagenesis (Curtis et al. 2011). Organic-matter porosity is often correlated to TOC (Alqahtani and Tutuncu 2014, Lu et al. 2015) and thermal maturity (Ma 2016). Organic-rich shales with high TOC and thermal maturity often have high organic-matter porosity because the conversion from kerogen to hydrocarbons often leads to an increase in porosity and permeability.

2.6 Digital Rock Physics (DRP)

Traditional characterization methods commonly used to assess porosity and permeability, such as nuclear magnetic resonance (NMR) and mercury injection capillary pressure (MICP) developed for conventional reservoirs, are insufficient for characterizing unconventional reservoirs. They have been reported to be expensive, inaccurate, incomplete, and time-consuming to complete, requiring months or even years for characterization of a single well site (Nelson 2009). Their applicability for highly heterogeneous unconventional reservoirs is limited. Therefore, the data obtained by these techniques may be biased and highly uncertain (Bertoncello and Honarpour 2013). This adds to the difficulties of exploration and production, and has caused researchers to search for a new solution to supplement the existing characterization techniques.

Many modern researchers are now turning to the technique of digital rock physics as a potential solution for multiscale characterization of heterogeneous petroleum geomaterials, owing to the power of modern microscopes to reliably and precisely image various rocks (Curtis et al. 2012, Curtis 2014, Goral et al. 2016, Loucks et al. 2009, Saraji 2014, Tono 2008, Wang 2014).

Increased interest in shale oil and gas reservoir characterization has sparked novel approaches to reservoir rock analysis, incorporating many modern scientific digital two-dimensional (2D) or three-dimensional imaging techniques, such as micro- and nano-X-ray microscopy, focused ion beam scanning electron microscopy, and (scanning) transmission electron microscopy (S/TEM), among others. Recent advancements in X-ray and electron microscopy provide a tremendous opportunity for surveying rock samples and

zooming in to capture the intricate nature of heterogeneous and nanostructured geomaterials (Blunt et al. 2013, Lopez et al. 2012, Zhang et al. 2011).

Despite the abilities of each technique to image structures across particular magnification ranges, these scientific digital imaging methods, individually, are limited by the sample size or imaging resolution and no single technique is capable of fully capturing the multiscale heterogeneity of a shale rock. A major challenge in the proper identification and characterization of reservoir heterogeneity is the need for balance between inspection volume and spatial resolution. Any characterization approach must incorporate sufficient resolution to identify nanometer scale features while being able to survey how these features relate to the larger-scale volumes, on the scale of hundreds of microns to millimeters and beyond.

To this end, a sequential investigation at different scales, using multiple techniques, is necessary to bridge a range of scales and properly characterize and correlate distributions of the shale microstructural properties. Therefore, this study illustrates the concept of coupled XRM and FIB-SEM analysis as a correlative approach for 3D investigation of heterogeneous shales to provide a representative and uniquely informative perspective on rock properties (Knackstedt et al. 2012).

2.6.1 X-ray Microscopy (XRM)

X-ray imaging systems, or X-ray computed tomography (XCT) scanners, have historically been very important to reservoir characterization because of their unique abilities to acquire 3D images of rock specimens at various scales and resolutions. The nondestructive nature of the technique allows specimens to be physically preserved

during imaging, retaining them for subsequent analytical or image-based analysis (Goldstein et al. 1981, Merkle et al. 2014).

In the XCT technique, several 2D projection radiographs are collected while rotating the specimen through 180° (“parallel-beam” configuration) or 360° (“cone-beam” configuration). These projection radiographs are reconstructed using standard procedures, such as filtered-back projection or Feldkamp-Davis-Kress (FDK), to produce digital, 3D volumetric representations of the structure of the specimen (Herman 2009). The different gray scale values, or computed tomography (CT) numbers, found within the reconstruction volumes, correspond to different X-ray absorption rates, which incorporate localized compositional and structural heterogeneities as well as mass-absorption coefficient for each material.

X-ray microscopy expands on the traditional CT techniques and incorporates X-ray optics, such as a tunable detection system, providing high spatial resolutions across a range of specimen sizes (Merkle and Gelb 2013). It is used for many different types of reservoir rocks and has recently gained favor for mudstones, due to resolution improvements in the instrumentation (Gelb et al. 2011). The maximum spatial resolution ranges to the sub-micron regime for specimen sizes into the tens of millimeters and has demonstrated resolution to the tens of nanometers for specimen sizes in the tens of microns. The XRM technique has demonstrated many unique advantages for localized 3D characterization without disturbing the specimen structure, which has increased its popularity for DRP applications (Gelb et al. 2012).

2.6.2 Focused Ion Beam Scanning Electron Microscopy (FIB-SEM)

XRM alone provides access to data across a unique range of length scales, but is not sufficient to characterize the smallest features of the rock microstructure. For this reason, SEM has grown in popularity in recent years as a technique to capture, for example, the smaller pores in shale (Huang et al., 2013). Commercial SEM systems can provide spatial resolutions on the order of single nanometers, which represent an important length scale for understanding fluid transport dynamics. SEM alone, however, only provides 2D information, and it is often the 3D nature of these features that is of interest to DRP modeling protocols (e.g., pore connectivity). This has led to novel approaches for 3D SEM.

The combination of focused ion beam (FIB) systems with high-resolution scanning electron microscopes has grown in popularity in recent years for high-resolution analysis of localized 3D volumes. The FIB-SEM technique relies on using a focused ion beam to polish away a thin (~10 nm) layer of material, exposing a layer below the original front surface of the specimen. A high-resolution field-emission SEM is used to image the structure, and then the process is repeated. This gives rise to a serial-sectioning approach to 3D imaging, as the layers may be digitally assembled into a 3D representation for subsequent analysis and modeling (Figure 2.6). Using this method, 3D imaging with resolution of a few nanometers has been made possible, leading to new insights into rock fabric, porosity, and permeability (Lemmens et al. 2011). This allows for accurate characterization of shale rock and for direct modeling and simulation of flow in the 3D datasets, with resolutions on the order of single nanometers.

2.6.3 XRM/FIB-SEM Correlative Microscopy

The flexibility of the FIB-SEM imaging system is high, but it has two unfortunate drawbacks. The technique is both destructive and highly localized. Nevertheless, this method of 3D reconstruction gives access to a variety of valuable microstructural information and may be extended to chemical information using correlative energy-dispersive X-ray spectroscopy (EDS). Although the resolution for this technique lies in the single nanometers, the volumes have historically been correspondingly small and often not representative of overall rock properties, so some guidance is necessary prior to 3D imaging with FIB-SEM. In other words, to make the FIB-SEM technique most effective, it must be directed using some “a priori” knowledge. For this reason, the current state-of-the-art digital rock laboratories are turning toward a correlative technique, using XRM and FIB-SEM in concert to survey a material, identify a region of interest (ROI) for further inspection, and then localize with higher resolution, all in 3D. This allows the unique strengths of both X-ray and electron microscopy to be effectively used together, for an accurate characterization of the sample. In cases of highly heterogeneous formations, such as shale reservoirs, this correlative technique suggests an efficient future pathway for digital rock investigations.

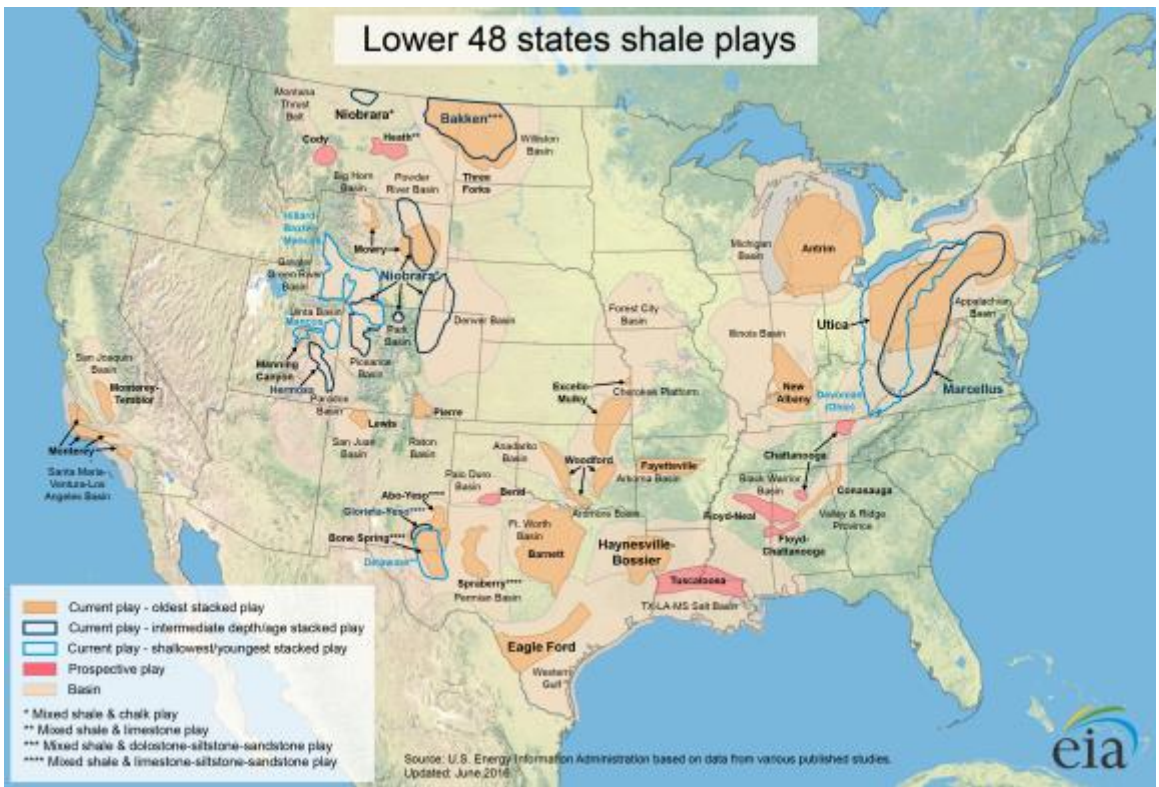


Figure 2.1. Shale oil and gas plays in the United States. Source: U.S. Energy Information Administration (EIA) Annual Energy Outlook 2014.

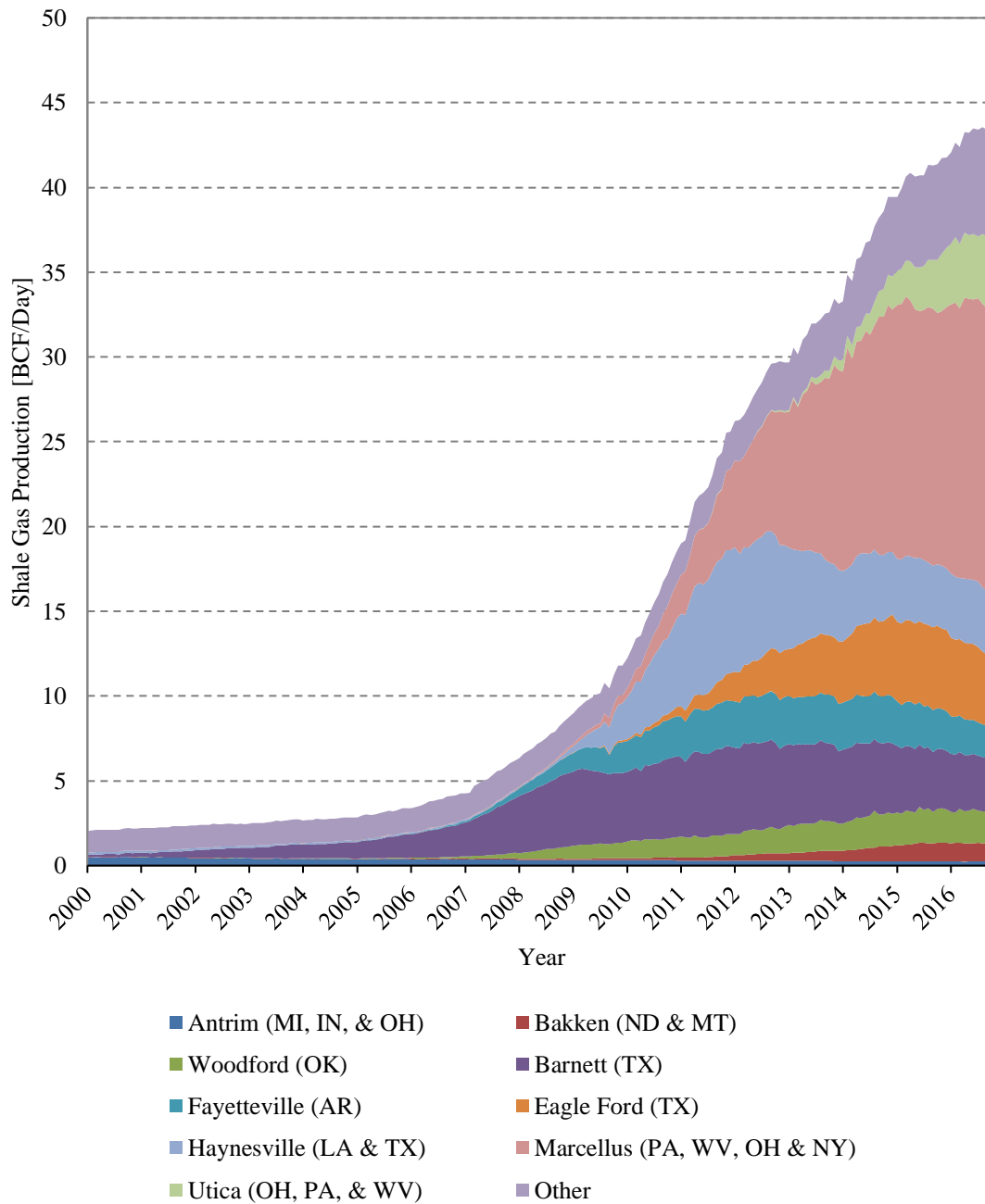


Figure 2.2. Shale gas production from selected plays in the United States through the years 2002-2016. Source: U.S. Energy Information Administration (EIA) Annual Energy Outlook 2014.

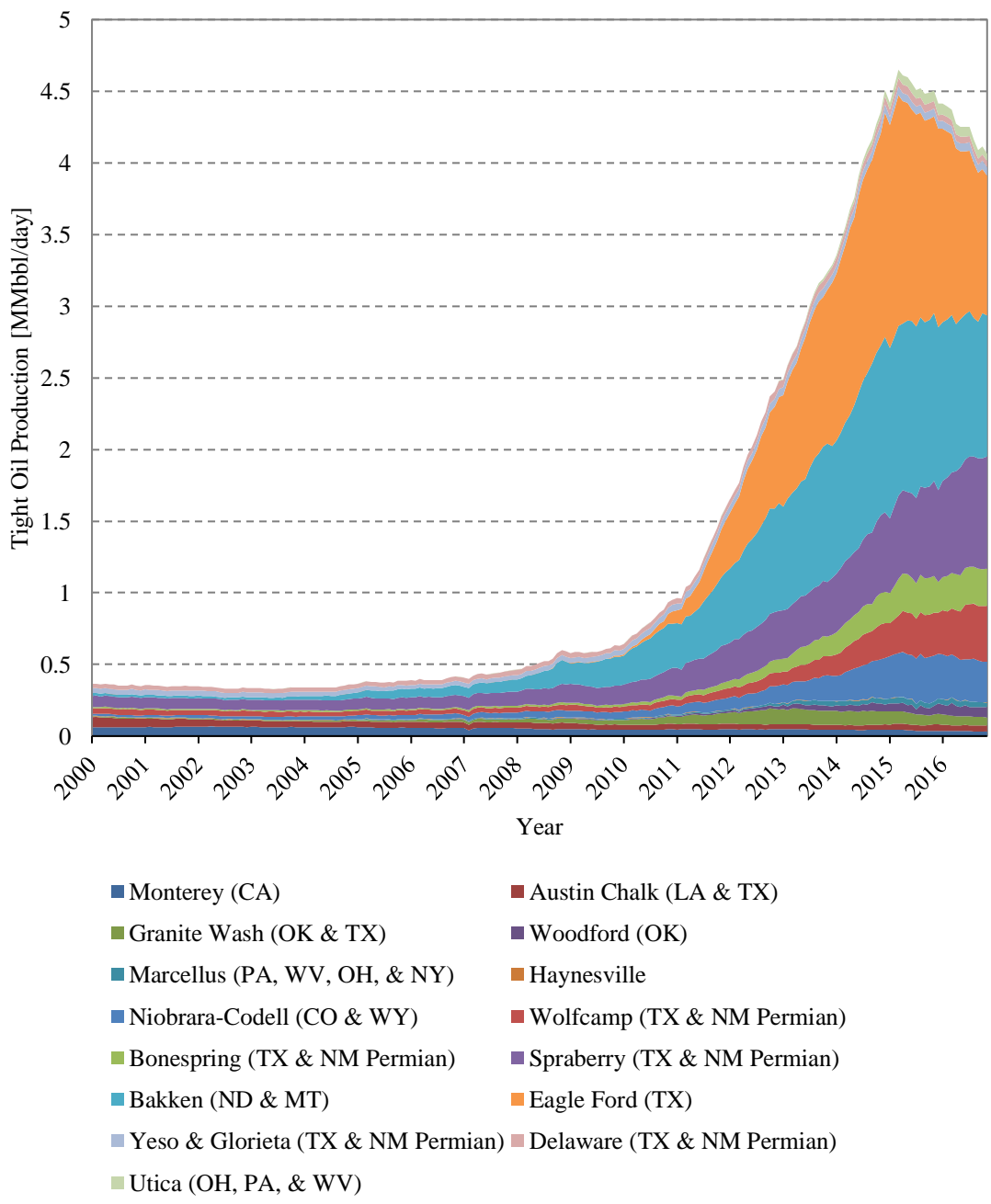


Figure 2.3. Tight oil production from selected plays in the United States through the years 2002-2016. Source: U.S. Energy Information Administration (EIA) Annual Energy Outlook 2014.

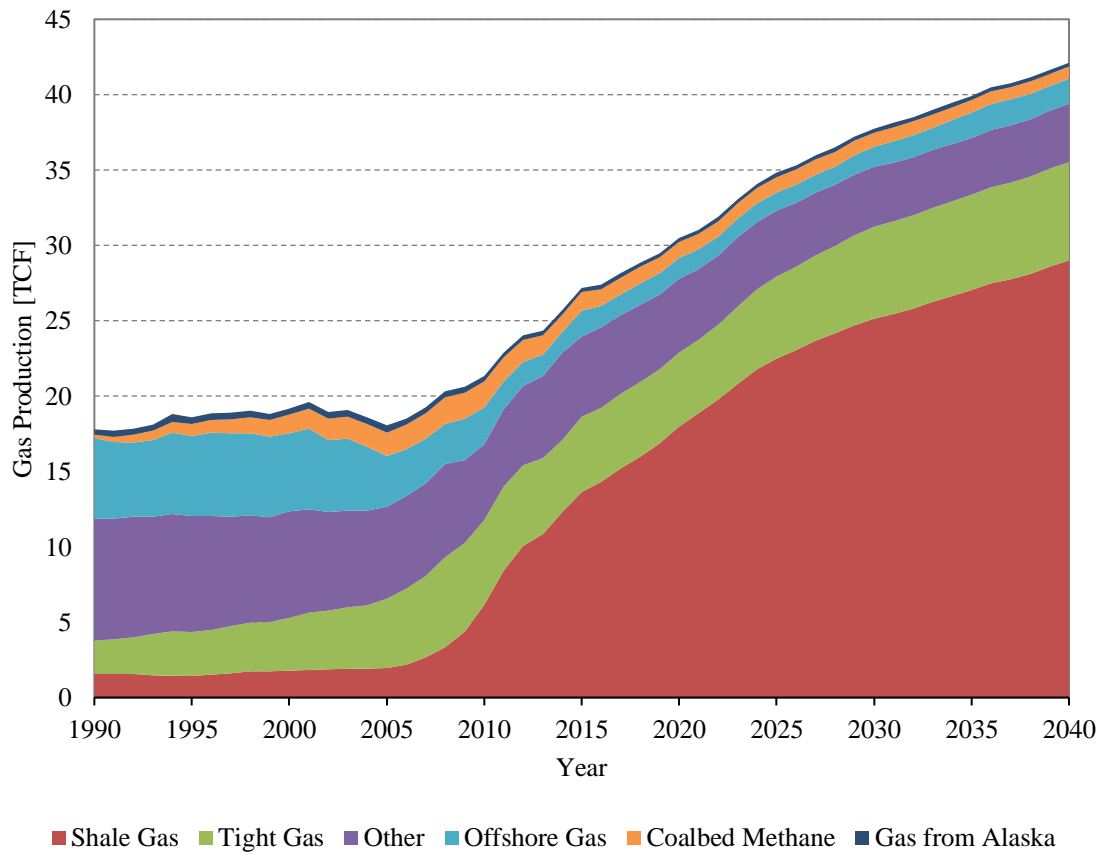


Figure 2.4. Dry natural gas production by source in the United States through the years 1990-2040. Source: U.S. Energy Information Administration (EIA) Annual Energy Outlook 2014.

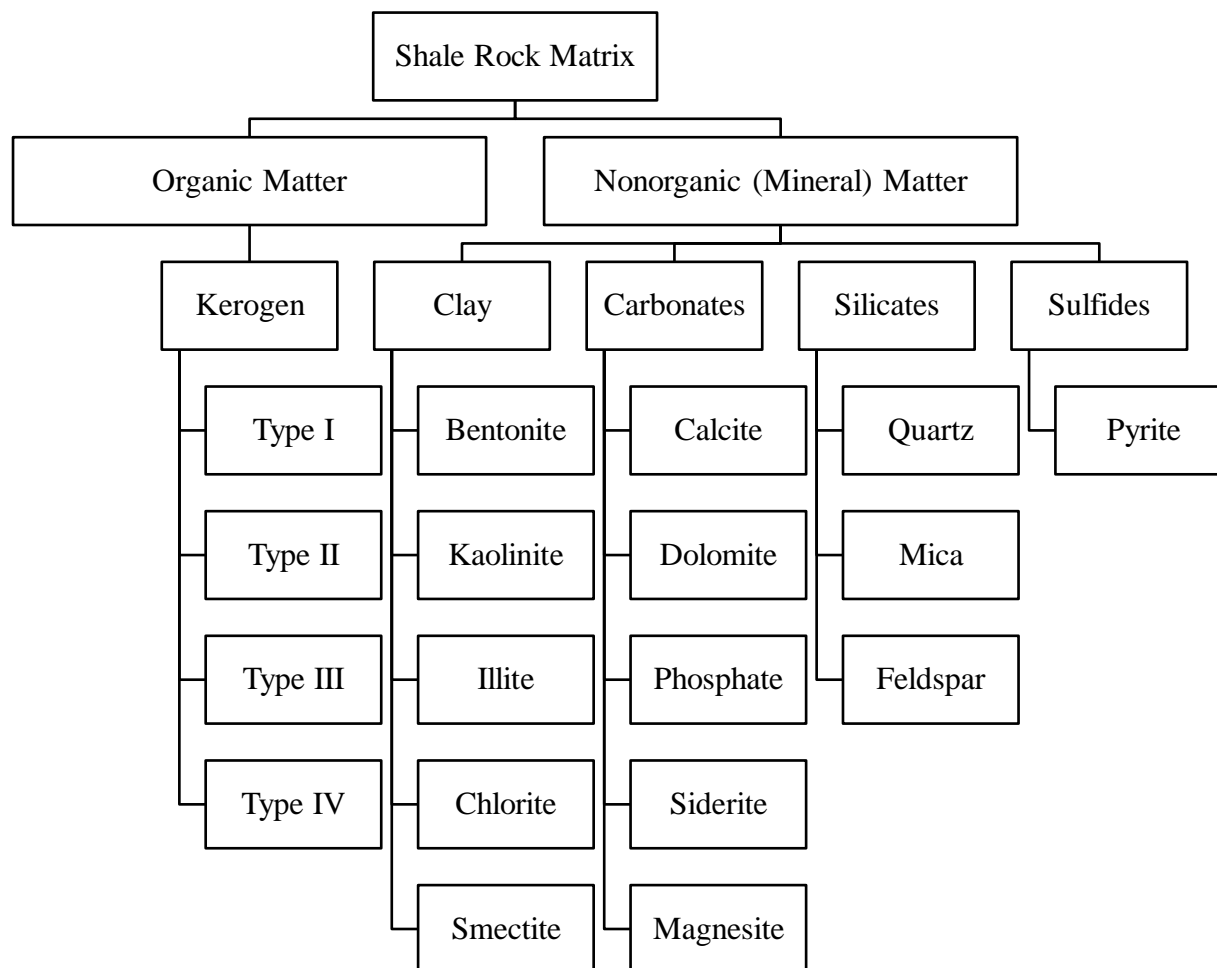


Figure 2.5. Shale rock matrix composition classification.

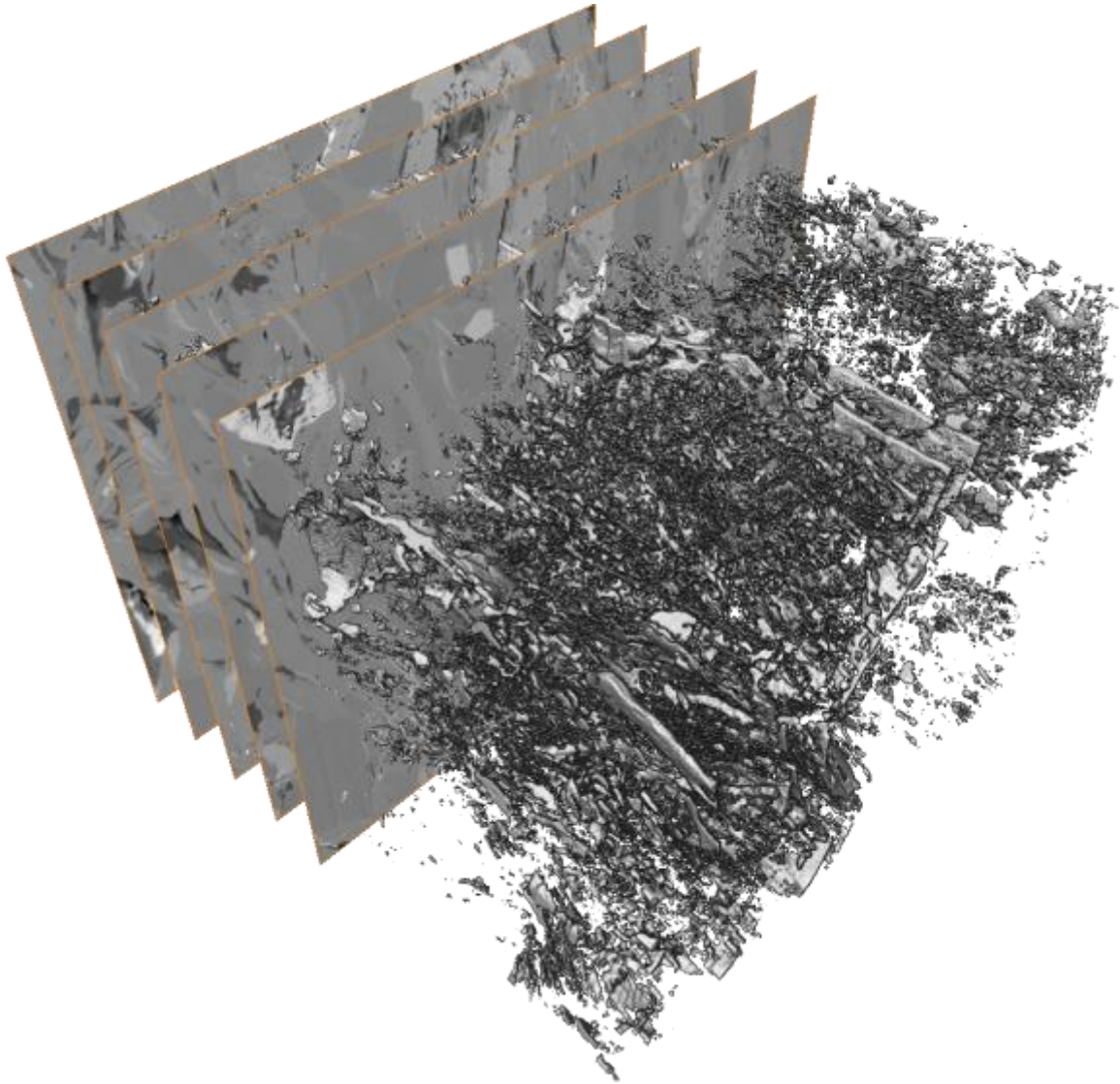


Figure 2.6. Focused ion beam (FIB) scanning electron microscopy (SEM) serial-sectioning.

CHAPTER 3

RESEARCH STATEMENT

The heterogeneity associated with complex shale reservoir pore systems has broad implications on the development of the unconventional oil and gas industry. Recent studies have indicated that shale pores significantly vary in number, size (from nano- to micropores), and classification (organic and nonorganic pores). Thus far, the role of pore network and, more specifically, what pores contribute the most to the oil and gas storage, or to the production process, is not well understood and remains largely unknown. Hence, it is vital to determine how well different pores are connected and how they create possible flow pathways for hydrocarbon migration. Moreover, in the context of shale oil and gas production, factors, such as pore and fracture network architecture or fluid-rock interaction, are expected to significantly influence the hydrocarbons storage and transport mechanisms. There is a limited number of research studies focusing on either quantification of the geometry of individual pores and fractures, or modeling and simulation of the transport phenomena in nanostructured shale rock matrix based on the 3D high-resolution scientific digital imaging data.

Therefore, in this study, a comprehensive digital rock physics framework is presented for pore network modeling in the Woodford Shale and the Marcellus Shale rock matrix using correlative micro- and nano-X-ray microscopy and focused ion beam

scanning electron microscopy serial-sectioning. Properties of pore types and networks, together with estimates of pore connectivity, are investigated – organic and nonorganic pore systems are quantified as representative pore networks for future finite element modeling and simulation studies of continuum or non-continuum transport phenomena within heterogeneous petroleum geomaterials.

CHAPTER 4

METHODS

The Woodford Shale and the Marcellus Shale are important hydrocarbon source rocks and are recognized as two of the "magnificent seven" along with the Barnett, Fayetteville, Haynesville, Horn River, and Montney. Horizontal drilling and hydraulic fracturing tandem have made the Woodford Shale and the Marcellus Shale formations prolific and self-sourced unconventional reservoirs that yield both gas and liquids.

The Woodford Shale formation produces gas, condensate, and oil at thermal maturities from mature ($>0.5\%$ R_o) to postmature (2-3% R_o). The Devonian organic-rich Woodford Shale's bulk organic matter type is type II kerogen (Cardott 2012).

The Devonian Marcellus Shale from Appalachian Basin contains one of the largest world-class shale gas plays in North America. It is divided into two members, more organic-rich lower Marcellus (Union Springs Shale) and less organic-rich upper Marcellus (Oatka Creek Shale), which are separated by the Cherry Valley and Purcell Limestones (Zagorski et al. 2012). Thermal maturity (vitrinite reflectance) of the black shale of the Appalachian Basin is $R_o = 1.6$ and above throughout most of the play, and total organic carbon (TOC) is 2-10% (Bruner and Smosna 2011). The Marcellus Shale contains both marine liquids-prone Type II kerogen and terrestrial gas-prone Type III kerogen (Chen et al. 2015).

The location information of the Woodford Shale (Woods County in Oklahoma) (provided by U.S. Geological Survey (USGS) Core Research Center) and (Oatka Creek) Marcellus Shale (Green Country in Pennsylvania) (provided by National Energy Technology Laboratory (NETL)) samples used in this study is given in Table 4.1.

4.1 Sample Preparation for SEM and/or FIB-SEM

Both Woodford Shale and Marcellus Shale samples were first prepared for preliminary SEM imaging and analysis. The shale rock sample preparation procedure protocol is given below.

- a) First, we cut the rock with a mechanical saw at 200-250 RPM to the desired size and attach it to a SEM stub. Alternatively, rock cuttings can be submerged into epoxy resin to avoid later fracture creation. Later, we let the sample dry under vacuum (to avoid bubble creation).
- b) Second, we mechanically polish the shale rock sample surface with a sequence of silicon carbide paper. We start with 60 grit (260 micron), and then proceed with finer grits of 600 (26 micron), 800 (22 micron), and 1200 (15 micron). Subsequently, we mechanically polish the shale rock sample surface with 3 micron and 1 micron diamond lapping film discs. We use kerosene as a lubricating and cooling media during this operation.
- c) Third, we let the sample dry in an oven in approximately 200 °C.
- d) Next, if available, we mill the top surface of the shale rock sample with an argon ion beam milling device. This corresponds to approximately 0.05 micron diamond lapping film disc mechanical polishing. Sheer force-free milling allows for an

- artifact-free surface. We set the right and left beams to 4 kV voltage, 45% focus, and 4° beam angle, as shown on Figure 4.1. We mill for approximately 1.5 hours.
- e) Shale rock is a nonconductive sample that charges during the SEM analysis. Therefore, to avoid charging effect, we coat the sample with about 10-20 nm of carbon. The deposited carbon thickness typically does not affect SEM analysis but keeps the sample from accumulating charge and drifting.

4.2 XRM/FIB-SEM Correlative Microscopy for the Woodford Shale and the Marcellus Shale

4.2.1 Case Study I: The Woodford Shale

The Woodford Shale sample was imaged several times using XRM at successively higher magnifications (higher resolutions with correspondingly smaller characterization volumes), and then finally imaged by FIB-SEM serial-sectioning. As described below, at some stages the specimen was imaged intact, and at other stages the sample was milled to a smaller size to increase the achievable spatial resolution. Figure 4.2 summarizes the correlative (nano and micro) X-ray and scanning electron microscopy workflow for the Woodford Shale.

4.2.1.1 Micro-XRM

The end trim of a 25 mm core plug was mounted to a sample holder for 3D imaging with micro-XRM (Figure 4.3). This microscope achieves tunable spatial resolution by using a system of visible light objective lenses, each coupled to a scintillating screen, which allows a range of different magnifications to be achieved

without further trimming to the specimen. Three-dimensional datasets were produced by collecting a series of 2D X-ray projection radiographs, which provided 3D volumetric data using an FDK reconstruction algorithm. The XRM detection system is capable of producing volumetric data up to $2048 \times 2048 \times 2048$ voxels, but in the present experiment, the pixel size was binned to a $1024 \times 1024 \times 1024$ volume to increase the effective throughput in the experimental data.

The initial XRM experiments were carried out in three stages. In the first stage, data from the entire 25 mm diameter plug were captured using a 0.4X objective lens, which was tuned to provide a voxel size of 29 μm . This allowed inspection of the long-length scale features, in order to inspect the specimen for bulk heterogeneity and select smaller regions for higher-resolution investigation. From this dataset, a region that appeared to represent the specimen as a whole was identified and optically enlarged. A 4X objective was used for this subsequent scan with a voxel size of 2.5 μm , collecting data through a cylindrical volume of 2.5 mm in each dimension. This second scan used the technique of interior tomography, where the specimen was left as an intact 25 mm plug, to eliminate any potential errors introduced by specimen preparation on the higher-resolution data.

4.2.1.2 Nano-XRM

To achieve higher throughput for characterizing features on a smaller length scale, a nano-XRM (Figure 4.4) was used. This instrument is capable of providing down to 50 nm spatial resolution for suitably prepared samples, with a switchable “large field of view” mode that provides 150 nm resolution across a 65 μm isotropic volume. The

nanoscale XRM system necessitates a smaller sample geometry, for which an Oxford Lasers laser ablation system (Figure 4.5) was employed. The laser milling process provides nonmechanical material removal, minimizing the chances of additional fractures being introduced in the sample preparation. Using parameters provided by the manufacturer to minimize damage caused by localized heating, a cylindrical pillar ~100 μm in diameter was created at the top surface of the end trim. This specimen was characterized following a similar procedure of radiograph collection and 3D reconstruction using the large field of view mode (200X magnification), resulting in a cylindrical data volume 65 μm in each dimension on a $1024 \times 1024 \times 1024$ voxel volume (64 nm voxel size).

Figure 4.6 presents correlative (micro and nano) X-ray microscopy (XRM) workflow. Nano- and micro-XRM 3D models are visualized by the ORS Visual SI software.

4.2.1.3 FIB-SEM

Although the XRM volumes provided data across a range of length scales, still finer features were suspected based on prior research (Bai et al. 2013). To continue the nanoscale investigation, a correlative microscopy approach was employed using the Atlas 5 software platform. The specimen was transferred to a SEM equipped with a high-current FIB (Figure 4.7). Using 100 nA milling current on the FIB, the upper mass on the pillar was milled away until the same volume captured in the nanoscale XRM was reached. After locating a suitable region of interest, the site was prepared for FIB-SEM serial-sectioning by standard methods. Approximately 3000 serial images were then

collected in a single-batch acquisition spanning a total depth greater than 21 μm , with each image capturing a 40 μm \times 10 μm field of view. To observe nanoporosity in the organic matter, a voxel size and slice thickness of 7 nm were selected, resulting in an image stack comprised of approximately 5700 \times 1800 \times 3000 voxels.

The rapid data acquisition rate was possible because each section was imaged with the SEM sequentially with FIB milling. Furthermore, a duplex signal was collected for each section. As the electron beam was rastered across the surface, dwelling briefly on each pixel, the secondary electron signal was acquired with the secondary electron secondary ion (SESI) detector and the backscattered electron signal was simultaneously acquired with the energy-selective backscatter (EsB) detector. The complementary information from these two signals was then blended into a single image to optimize contrast across various minerals, organic bodies, and matrix pores.

4.2.2 Case Study II: The Marcellus Shale

Similarly to the Woodford Shale sample, in order to characterize the Marcellus Shale sample at various length scales and identify the region of interest (ROI), a correlative microscopy approach was employed incorporating a nondestructive nano-X-ray microscopy and destructive focused ion beam scanning electron microscopy serial-sectioning. Due to limited time and budget, only nano-XRM and FIB-SEM were used to image and analyze the Marcellus Shale sample (Figure 4.8).

4.2.2.1 Nano-XRM

A 1 mm mini plug was prepared from a 12 mm x 12 mm x 3 mm cuboid of Marcellus Shale using an Oxford Lasers laser ablation system. The laser ablation system utilized a 2.5 W, 532 nm pulsed laser, designed to minimize the depth of rock affected by the heat of the laser. From this 1 mm mini plug, a 65 micron diameter pillar was created using the same sample preparation tool.

The 65 micron pillar was then imaged with nano-XRM, creating a 3D dataset comprised of 65 nm voxels, with a spatial resolution of 150 nm. The emission from a 5.4 keV chromium source was focused onto the sample via capillary condenser lens and X-ray transmission through the sample, measured at different specimen rotation angles, was magnified using a Fresnel zone plate X-ray lens. The resulting image was further magnified with a scintillator-coupled visible light objective, producing a signal that was captured by a 16-bit CCD camera. As the sample rotated through 180°, 901 two-dimensional X-ray radiographs were captured. The resulting computed tomography radiograph acquisitions were reconstructed using a filtered back projection algorithm to create a 3D dataset (Tkachuk et al. 2007).

4.2.2.2 FIB-SEM

Using the nano-XRM data to prescriptively navigate to a volume within the 65 μm pillar that required higher resolution imaging, a 22 μm x 22 μm x 10 μm volume was imaged with FIB-SEM using 10 nm/voxel at 1.5 kV.

Table 4.1. Woodford Shale and Marcellus Shale samples' location information.

Formation Name	Woodford	Marcellus
Well Latitude	36.794039 N	38.818654 N
Well Longitude	98.903786 W	80.169192 W
Sample Depth	1982 m	2390 m

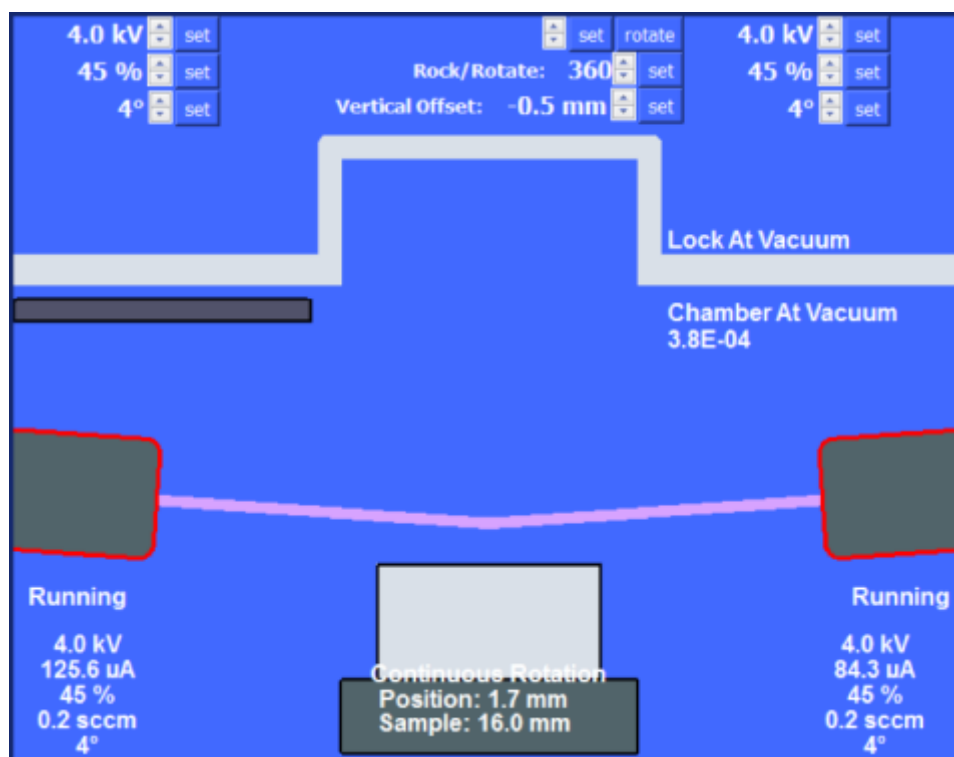


Figure 4.1. Sample preparation with argon ion beam milling system.

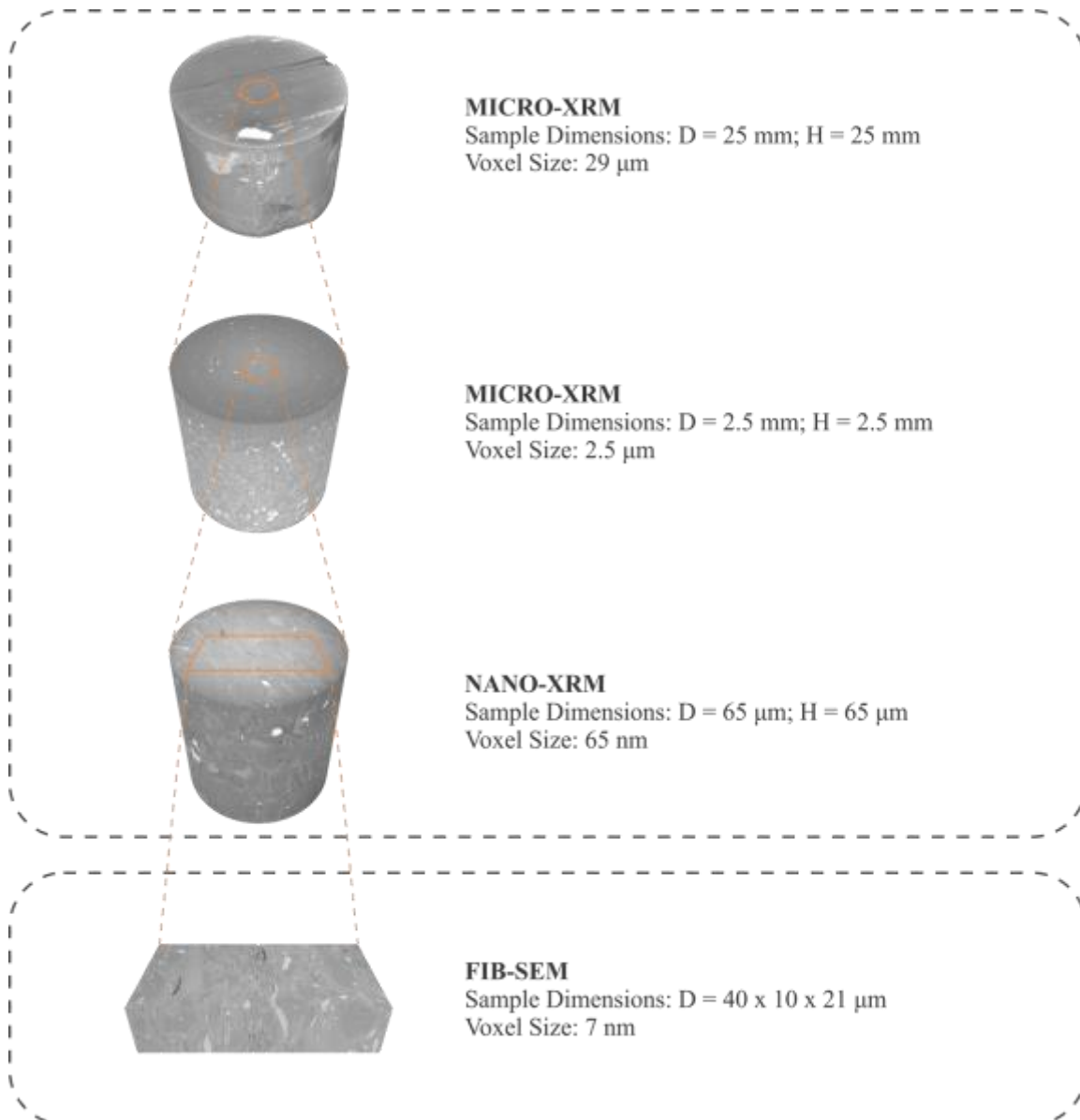
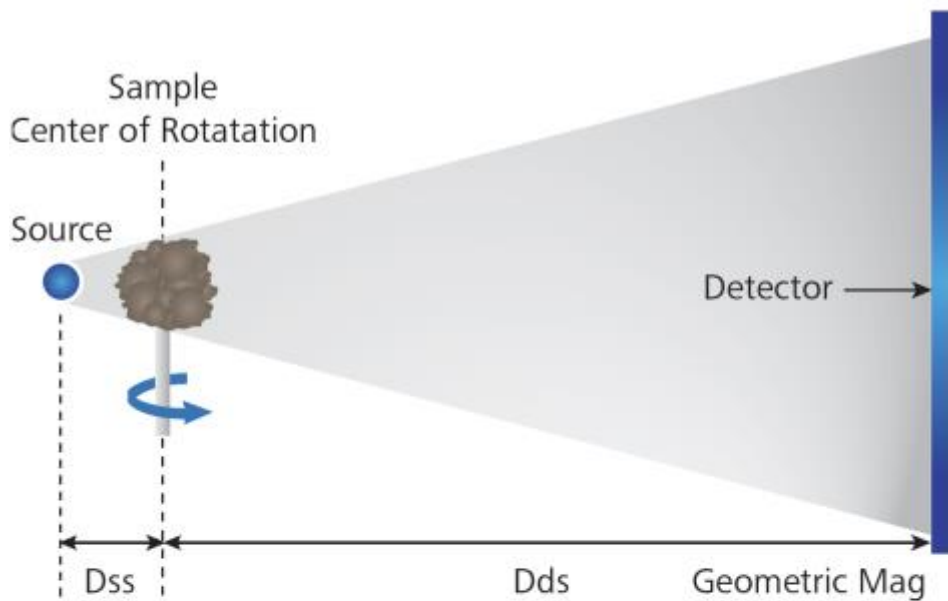


Figure 4.2. Correlative micro-X-ray microscopy (micro-XRM), nano-X-ray microscopy (nano-XRM), and focused ion beam scanning electron microscopy (FIB-SEM) workflow for the Woodford Shale.

Conventional Micro-CT Architecture



ZEISS XRM Two-stage Magnification Architecture

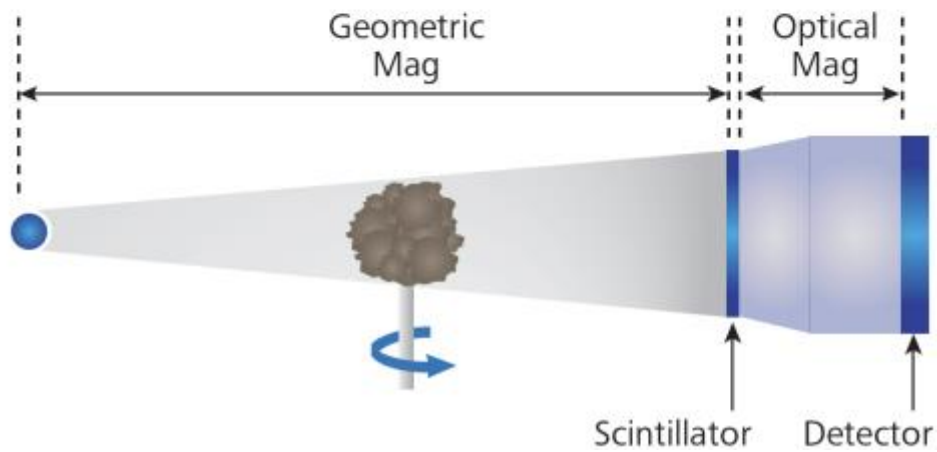


Figure 4.3. Schematic diagram illustrating the principles of operation of micro-X-ray microscope (micro-XRM). Reprinted with permission from Carl Zeiss Microscopy GmbH.

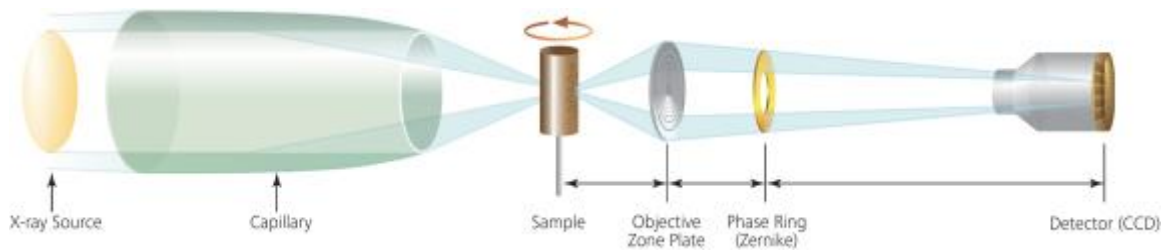


Figure 4.4. Schematic diagram illustrating the principles of operation of nano-X-ray microscope (nano-XRM). Reprinted with permission from Carl Zeiss Microscopy GmbH.

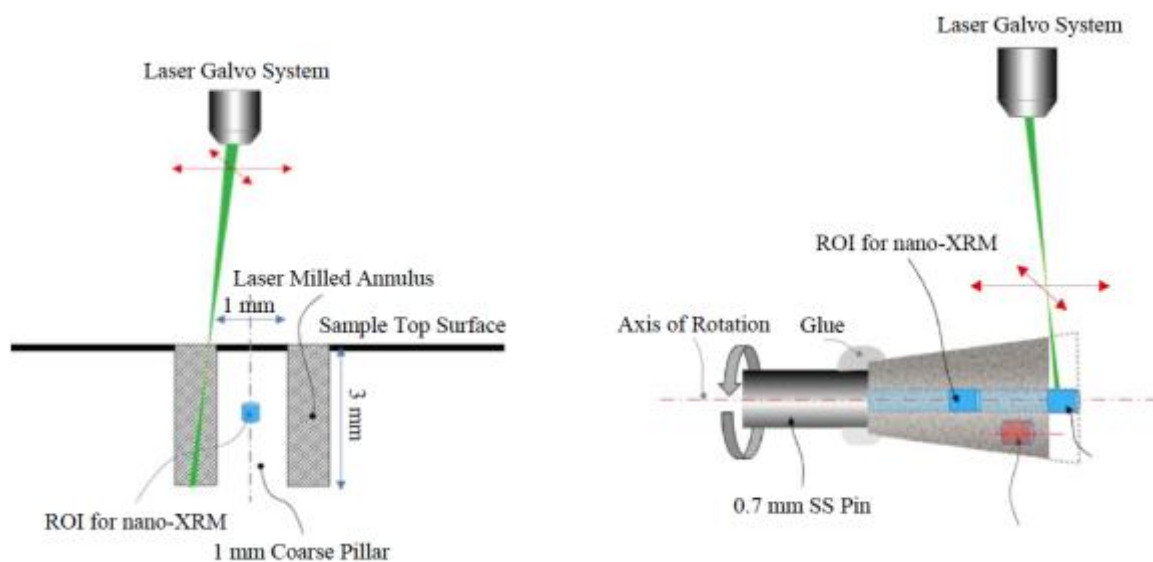


Figure 4.5. Sample preparation with laser ablation system (after Goral et al. 2015b).

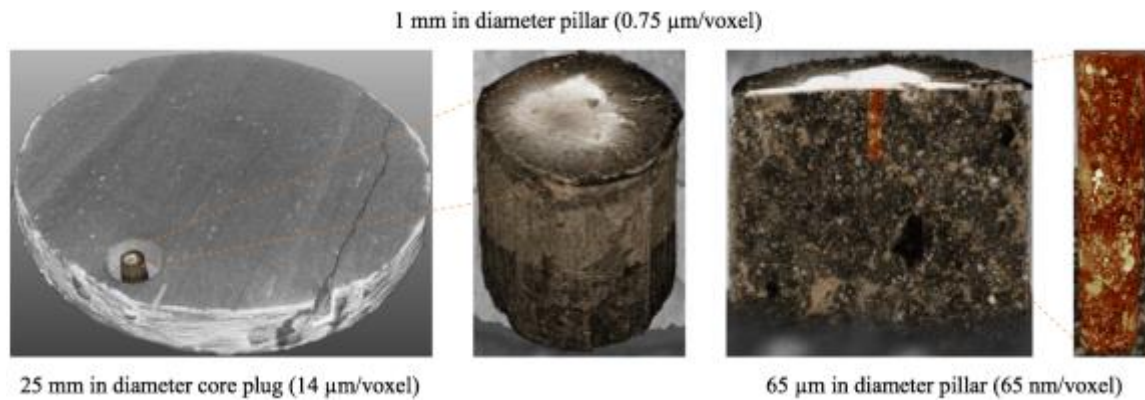


Figure 4.6. Correlative (micro and nano) X-ray microscopy (XRM) workflow for the Woodford Shale.

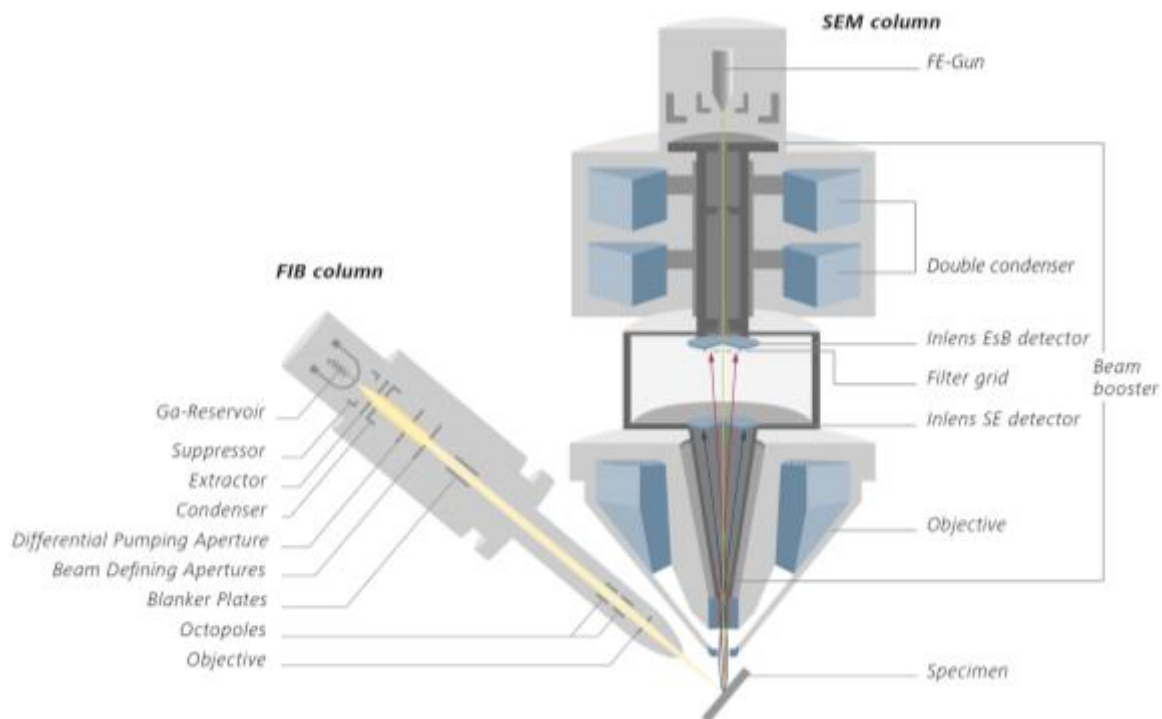


Figure 4.7. Schematic diagram illustrating the principle of operation of focused ion beam scanning electron microscope (FIB-SEM). Reprinted with permission from Carl Zeiss Microscopy GmbH.

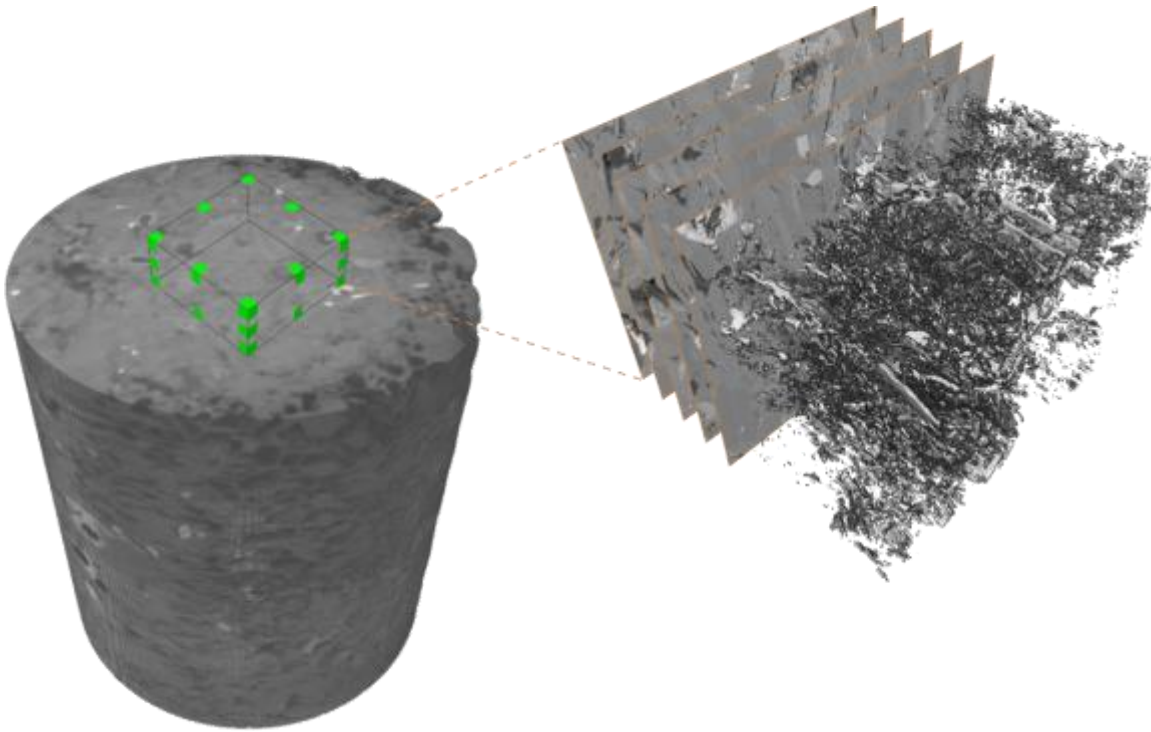


Figure 4.8. Correlative nano-X-ray microscope (nano-XRM) and focused ion beam scanning electron microscopy (FIB-SEM) workflow for the Marcellus Shale.

CHAPTER 5

RESULTS AND DISCUSSION

5.1 Case Study I: The Woodford Shale

The Woodford Shale sample was observed to be anisotropic and heterogeneous across a range of scales. Figures 5.1 and 5.2 provide scanning electron microscopy and automated mineralogy and petrography images of the sample, respectively. SEM imaging was performed in a SESI-EsB mode, so that grey levels on the flat shale surface vary with mean atomic number and thus correlate with different mineral phases. In Figure 5.1, black regions depict pores and micro-fractures, dark gray represents organic matter (kerogen), gray is silicate (feldspar, clay, quartz), light gray is carbonate (dolomite), and white objects are sulfide (pyrite). Figure 5.2 depicts a mineral and structural mosaic map of the shale rock sample. The QEMSCAN analysis showed presence of feldspar (88.6%), quartz (9.9%), dolomite (0.1%), and pyrite (1.4%) minerals. Both the SEM and automated mineralogy and petrography highlight a wide range of pore sizes and material properties without apparent spatial relationships within the specimen.

Shales exhibit microstructural and mineralogical heterogeneity over scales ranging from millimeters to nanometers. Thus, a multiscale characterization approach is required to provide a representative and uniquely informative perspective of sample properties. Any imaging procedure must balance the dual requirements of providing

sufficient resolution to identify characteristic microstructural features while also ensuring a sufficient characterization volume to represent the bulk microstructure. While X-ray and focused ion beam scanning electron microscopy can provide detailed images of rock matrix at the micro- and nanoscale, the high magnification required means that the total volume of the rock imaged is small, and therefore the results can be statistically questionable. It is thus very important to determine the sample volume size that must be examined to understand the oil or gas reserves contained in a shale reservoir, as the small features require a very high-resolution imaging system, which comes with limited field of view (Fogden 2014, Guan et al. 2011, Shearing et al. 2009). The ability to conduct imaging analysis over a variety of scales is therefore critical. However, establishing locations where imaging should be carried out remains a challenge, overshadowed only by the upscaling issues involved, when data are extrapolated to the reservoir-scale (Hooghan 2014). When performing nanometer scale examination of shale samples, it is important to consider the scale of the observation and the scale of interest. Image analysis provides a visual appreciation of the pore network in shales but is not yet a statistically valid method to evaluate shale oil and gas reservoirs (Chalmers et al. 2012). It is typical that a micron-sized volume is imaged, whereas a target interval may be on the order of kilometers. This unavoidably leads to concerns about taking representative samples and upscaling (Silin and Kneafsey 2011). Thus, to use 3D pore structure for analysis and simulation, the relative scale needs to be considered and intelligent volume selection, for example with XRM, may play a pivotal role in this analysis.

Figure 5.3 presents XRM reconstruction results. All three models present shale heterogeneity across different scales. Different features are seen in each of these models.

Figure 5.3a, made with micro-XRM (25 μm resolution), provides information about larger features (e.g., microfractures). However, pores are not visible. In Figure 5.3b, produced by micro-XRM at a higher resolution (2.5 μm resolution), some minerals start to be visible (pores are still not visible). Figure 5.3c, made with nano-XRM at 150 nm resolution, starts to resolve some of the bigger pores, but still the resolution is too low to resolve all of them, and they are difficult to discriminate from organics with this method.

Within these volumes, several tiny pores were observed, barely discernable at the best resolution of the XRM method. Although XRM images reveal the mineralized structure of shale, they cannot fully resolve the pore network of the sample. However, micro-XRM and nano-XRM were found to serve as a useful bridge from pore- to core-scale, which may further be used for correlation of all of the scales and, ultimately, for upscaling to the whole core and up to the entire reservoir.

The past decade has witnessed enormous advances in imaging software for image processing and analysis and image-based modeling and simulation. Equipped with 3D datasets from FIB-SEM, 3D digital rock models may be produced that represent the sample volume. Proper segmentation is the key to generating a 3D porosity network, as well as organic and mineral models. Segmentation is achieved by associating a phase with a specific range of gray levels in the 3D dataset and rendering the images into 3D block models (Figure 5.4). Visualizing the resulting models reveals the full detail of the rock geometry and material composition, hence providing important guidance to reconstruct real-world geometries, as well as templates for future simulation comparisons (Goral and Miskovic 2015, Takhar and Zhang 2009, Vega 2013).

It should be noted that image analysis of 3D datasets is, in itself, a challenging task as organic phases and pores may have similar gray levels. Porosity measurement has been found to be very sensitive to the threshold value. Improper segmentation can lead, for instance, to misidentification of organic material as pore space, resulting in overestimation of porosity and permeability (Schluter et al. 2014).

A FIB-SEM reconstructed and segmented model (performed at the same location as the nano-XRM) is better suited for investigation of the fine pore network structure. Figures 5.5a and 5.5b depict 3D models of organic and mineral matter, respectively, resulting from the FIB-SEM acquisition. A 3D pore network was then extracted to enable microstructure modeling and further simulations performed (Figure 5.5c). Having these high-resolution models, several important trends in the rock structure have been identified. Pore size distribution is strongly anisotropic, as expected for shale, and imaged porosity is equal to 1.56% (0.92% connected porosity). Segmentation of the Woodford Shale images revealed 2.69% and 95.75% of presumably organic and mineral matter, respectively. Note that the microcrack pores may be induced by coring or sample preparation, and may not be an in-situ feature, which may have influenced the porosity measurement.

5.1.1 Pore Network Modeling (PNM) in the Woodford Shale

Shale consists of organic and nonorganic (mineral) matter, and a variety of nanometer- to micrometer-sized pores.

There are four different pore types identified within the present study:

- Intraparticle organic-matter-hosted pore (located within a single organic particle),

- Intraparticle nonorganic-matter-hosted pore (located within a single mineral particle),
- Interparticle nonorganic-matter-hosted pore (located between mineral grains and crystals), and
- Interparticle non/organic-matter-hosted pore (located at the interface of organic and mineral phases).

An example of a 3D DRP model along with four main (organic and nonorganic) pore types embedded within shale rock matrix can be found in Figure 5.6. Thus far, the role of the pore network within this highly heterogeneous porous media is under investigation and has been a subject of many recent studies.

In this study, we present two general approaches for pore network modeling. We investigate both (non)organic-matter-hosted and (non)organic-matter-related pore systems. The two approaches slightly differ from each other and depend on organic-porosity interpretation. The first interpretation classifies organic-porosity as pores surrounded by the organic matter, while the second interpretation, alternatively, categorizes organic-porosity as pores attached to the organic matter. The reason for the need of both approaches is that the origin of these pores is unknown.

5.1.1.1 Organic- and Nonorganic-Matter-Hosted Pore Network

Modeling (PNM in the Woodford Shale

From the 3D datasets, one can obtain an understanding of the 3D pore network, its connectivity, and the location and distribution of organic and mineral phases. Therefore, the pore network has been separated into pores associated with organic and mineral

matter. Only pores surrounded by organic matter are classified as an organic-matter-hosted pore system. The remaining pores within the mineral matter and pores at the interface of organic and mineral phases are classified as nonorganic-matter-hosted porosity (Figure 5.7).

Estimated pore size (equivalent circular diameter) distribution showed that pores are 22.76 nm to 658.11 nm in diameter for the organic-matter-hosted pore network, as shown in Figure 5.8, and 19.89 nm to 1649.47 nm in diameter for the nonorganic-matter-hosted pore system (Figure 5.9). Therefore, it has been shown that the organic-matter-hosted pores are, in general, much smaller than the nonorganic-matter-hosted pores.

The resulting geometries of the organic-matter-hosted and nonorganic-matter-hosted connected pore networks were then skeletonized to identify the level of connectivity between pores and microcrack pores. The organic-matter-hosted and nonorganic-matter-hosted connected pore network models are shown in Figure 5.10.

The porosity of the nonorganic-matter-hosted and organic-matter-hosted pore systems is equal to 1.23% (0.81% effective porosity) and 0.33% (0% effective porosity), respectively.

5.1.1.2 Organic- and Nonorganic-Matter-Related Pore Network

Modeling (PNM) in the Woodford Shale

Later in this study, the Woodford Shale FIB-SEM model was separated into two regions, region I and region II, for comparison, eliminating a large microfracture through the center of the imaged region, suspected to be due to coring or sample preparation (Figure 5.11). Quantitative analysis of the 3D pore network models of a region I and

region II indicated a porosity of 0.66% and 0.55% for region I and region II, respectively, showing reasonable agreement between the two regions and suggesting that each volume was representative at the nanometer length scale. Percentages for each individual phase of both regions are given in Table 5.1 and 5.2.

Further, the pore networks of both regions were separated into pores associated with organic and nonorganic phases (Figure 5.12 and 5.13). Alternatively to the previous PNM classification, in this approach, any pore object adjacent to, or surrounded by, organic matter is classified as an organic-matter-related pore network.

Quantitative volumetric analysis revealed that 99.45% of the pores within region I and 81.53% of the pores within region II were connected to the organic phase, while the remaining pores were classified as nonorganic-matter-related pores. The difference in the organic-matter-related pore network fraction number between region I and region II comes from the difference in organic content within both regions, where the organic phase volume fraction accounted for 2.16% and 1.03% for region I and II, respectively.

5.2 Case Study II: The Marcellus Shale

Similar to the Woodford Shale, the Marcellus FIB-SEM dataset was processed, segmented, and reconstructed, using the Avizo software, into five different phases (pores, organic matter, silicate, carbonate, and sulfide) of the shale sample microstructure. The 3D reconstructions of organic and nonorganic matter are shown in the segmented images in Figure 5.14a and 5.14b, respectively. The 3D renderings of the shale volume reconstructed from serial-sectioning and imaging allow for quantitative analysis (voxel counts) of each phase volume and pore connectivity across the volume. The analysis

revealed 95.24% nonorganic content within the specimen. Organic content in this sample is relatively high at 2.32%. Quantitative analysis of the segmented 3D pore system image (Figure 5.14c) indicates a porosity of 2.44% with 1.12% of that being connected (Figure 5.14d). Volume fractions for each individual phase of the Marcellus Shale sample from the FIB-SEM study area are given in Table 5.3.

5.2.1 Pore Network Modeling (PNM) in the Marcellus Shale

5.2.1.1 Organic- and Nonorganic-Matter-Hosted Pore Network

Modeling (PNM) in the Marcellus Shale

The same as in the case of the Woodford Shale, porosity in the Marcellus Shale sample was observed to be prevalent in either the organic matter or the mineral matrix. Therefore, first, the pore network was separated into organic-matter-hosted and nonorganic-matter-hosted pores (Figure 5.15).

Similar to the Woodford Shale, it has been shown that the organic-matter-hosted pores are, in general, much smaller than the nonorganic-matter-hosted pores. Pores are measured to be approximately 22.55 nm to 438.88 nm in diameter for the organic-matter-hosted pore network, as shown in Figure 5.16, and 12.41 nm to 4324.53 nm in diameter for the nonorganic-matter-hosted pore system (Figure 5.17).

The resulting geometries of the organic-matter-hosted and nonorganic-matter-hosted connected pore networks were then skeletonized to identify the level of connectivity between pores and microcrack pores. The organic-matter-hosted and nonorganic-matter-hosted connected pore network models are shown in Figure 5.18.

The porosity of the nonorganic-matter-hosted and organic-matter-hosted pore systems are equal to 2.42% (0.93% connected porosity) and 0.02% (0% connected porosity), respectively.

5.2.1.2 Organic- and Nonorganic-Matter-Related Pore Network

Modeling (PNM) in the Marcellus Shale

Subsequently, the pore network is separated into pores associated with organic and nonorganic phases, namely organic- and nonorganic-matter-related porosity (Figure 5.19). Any pore object adjacent to, or surrounded by, organic matter is classified as an organic-matter-related pore network.

Quantitative analysis indicates organic-matter-related porosity of 1.93%, and nonorganic-matter-related porosity of 0.51%.

5.3 Woodford Shale vs. Marcellus Shale Reservoir Pore System

The pore network modeling study has shown that both the Woodford Shale and the Marcellus Shale consist of intraparticle organic- and nonorganic-matter-hosted pores, interparticle nonorganic (mineral) pores, and pores located at the interface of organic and mineral phases (interparticle non/organic-matter-hosted pores).

The results suggest that pores developed at the interface of organic and mineral phases strongly dominate over any other pore types within both the Woodford Shale and the Marcellus Shale FIB-SEM models. Interparticle non/organic-matter-hosted pore network has been demonstrated to have the potential for better connectivity than intraparticle organic- and nonorganic-matter-hosted pore systems.

Discontinuous pore networks, characterized by a large number of isolated pores, present a tremendous challenge for hydrocarbons production, as they are not effectively connected with existing natural or hydraulic fractures. This study, somehow, opens a door to more detailed study on three-dimensional heterogeneous shale reservoir pore systems, their connectivity, and their relationship with oil and gas production mechanisms.

Note that other shale-dominated formations will have their own characteristic pore systems and those pore networks may actually vary spatially within any shale reservoir. It is debatable whether the small volumes investigated in this thesis constitute a representative elementary volume (REV), but this is beyond the scope of this study, requiring much more detailed characterization of heterogeneity at all scales of the shale samples than is attempted here.

5.4 Image to Simulation Workflow for Continuum and Non-Continuum Transport

Phenomena in Heterogeneous Shale Reservoir Pore Systems

Shale reservoir pore systems are strong modifiers of sedimentary basin fluid dynamics and have a critical role in the distribution of hydrocarbons and containments of injected fluids (Bustin et al. 2008). Understanding the multiscale transport mechanisms between both organic and nonorganic pores and relatively larger fracture systems is of great importance for accurate predictions of hydrocarbon storage capacity and recovery rates (Chen et al. 2013, Shi et al. 2013, Solano 2014). It is well recognized that flow and transport processes in unconventional oil and gas reservoirs must be studied across multiple scales, and reservoir-scale simulations need to account for the impact of small-

scale heterogeneity (Geiger et al. 2012). In shale oil and gas reservoirs, the transport mechanism does not only follow the continuum Darcy's fluid flow equation, widely applied for conventional reservoirs (Alharthy et al. 2012, Amann-Hildenbrand et al. 2012, Collell et al. 2015, Darabi et al. 2012, Javadpour et al. 2007, Pathak et al. 2015b, Zhai et al. 2014). To describe the transport phenomena in ultra-tight porous media more accurately, a combination of continuum as well as non-continuum fluid flow modeling and simulation is required (Xia et al. 2017).

Having the representative shale reservoir pore systems, identified with X-ray and electron microscopy, we can now transform these pore networks into finite element models for any further continuum and non-continuum fluid flow modeling and simulation studies.

5.4.1 A Workflow for Continuum Fluid Flow in Heterogeneous Shale Reservoir Pore Systems

Large portions of connected pores and fractures from the volume shown in Figure 5.5d have been isolated as a network and can be further examined for continuum (e.g., fracture) flow properties. Therefore, the 3D geometry of the Woodford Shale's pore/fracture network was meshed to a tetrahedron volume mesh. The mesh was further simplified to reduce the computational cost of further simulation. The mesh resulted in 113,910 cells with mean edge length of 130 nm (Figure 5.20).

5.4.2 A Workflow for Non-Continuum Fluid Flow in Heterogeneous Shale Reservoir Pore Systems

A critical step in performing non-continuum (e.g., pore) fluid flow simulation is identification and extraction of a representative ROI. Due to the structural complexity and high level of detail of the reconstructed sample, as well as extremely high computational costs, fluid flow modeling and simulation over the entire pore network model is not practical. To overcome this limitation and provide a viable domain for numerical simulation, a box with dimensions of $1\ \mu\text{m} \times 1\ \mu\text{m} \times 2\ \mu\text{m}$ is selected from the FIB-SEM model of the Woodford Shale.

Importantly, having the information regarding nonorganic/organic content surrounding pore geometries, as shown in Figure 5.21, we can adequately assign boundary condition properties to realistically reflect the subsurface reservoir conditions that may significantly affect, for example, fluid-rock interaction.

Next, the pore geometry of the Woodford Shale is meshed to a tetrahedron volume mesh. The mesh resulted in 40,000 cells, for pore network, with mean edge length of 20 nm. Table 5.4 provides meshed three-phase (pore network, organic matter, and nonorganic matter) $1\ \mu\text{m} \times 1\ \mu\text{m} \times 2\ \mu\text{m}$ ROI of the Woodford Shale rock sample.

The presented image-to-simulation framework provides a viable tool for discretization and modeling of complex nanoscopic features identified using XRM and FIB-SEM. Structural information generated using this approach may be further utilized as a high-fidelity computational domain for studies of multiscale transport phenomena in heterogeneous petroleum geomaterials.

Table 5.1. Phase separation and quantification of the focused ion beam scanning electron microscopy (FIB-SEM) model of the Woodford Shale of the region I.


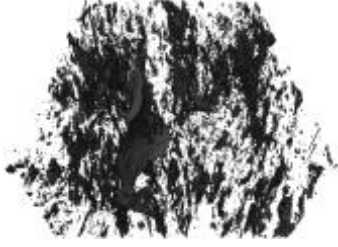

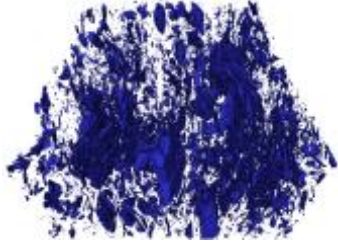
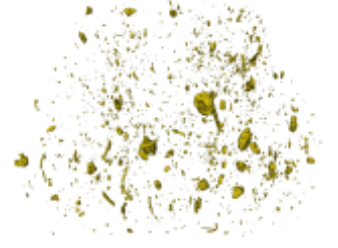
Phase		Fraction	
Pore Network		0.66%	
Organic Matter		2.16%	
Nonorganic Matter	Silicate	91.66%	
	Carbonate	5.17%	
	Sulfide	0.35%	

Table 5.2. Phase separation and quantification of the focused ion beam scanning electron microscopy (FIB-SEM) model of the Woodford Shale of the region II.

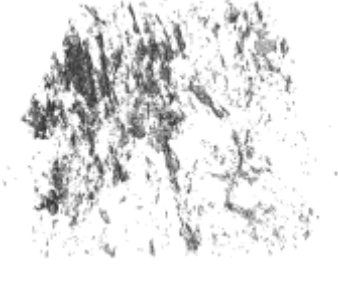

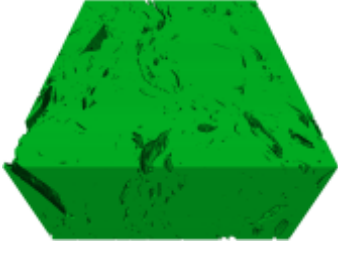
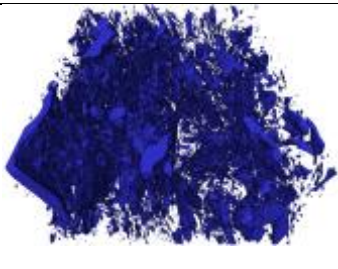
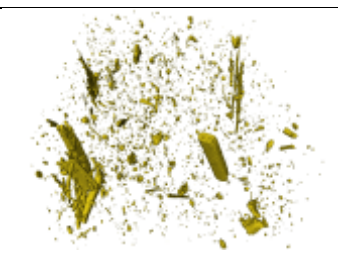
Phase		Fraction	
Pore Network		0.53%	
Organic Matter		1.03%	
Nonorganic Matter	Silicate	90.57%	
	Carbonate	7.34%	
	Sulfide	0.53%	

Table 5.3. Phase separation and quantification of the focused ion beam scanning electron microscopy (FIB-SEM) model of the Marcellus Shale.

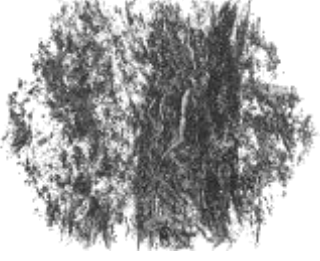
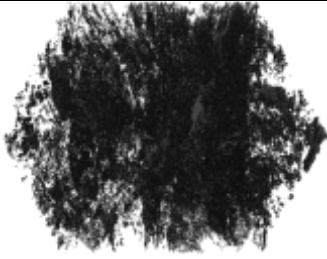
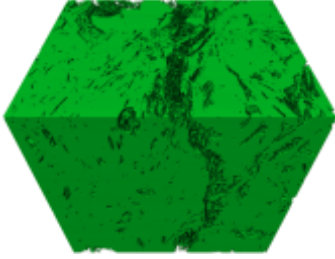

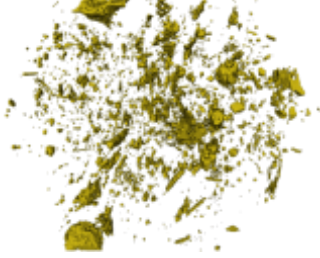


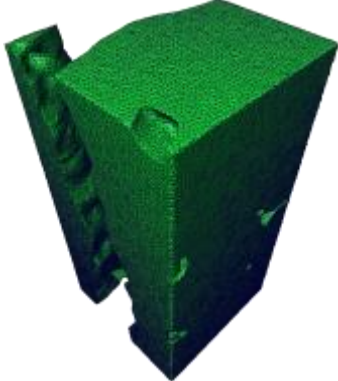
Phase		Fraction	
Pore Network		2.44%	
Organic Matter		2.32%	
Nonorganic Matter	Silicate	83.06%	
	Carbonate	10.96%	
	Sulfide	1.22%	

Table 5.4. Tetrahedron volume mesh of the pore network, organic matter, and nonorganic matter.

Phase	Tetrahedron Volume Mesh
Pore Network	
Organic Matter	
Nonorganic Matter	

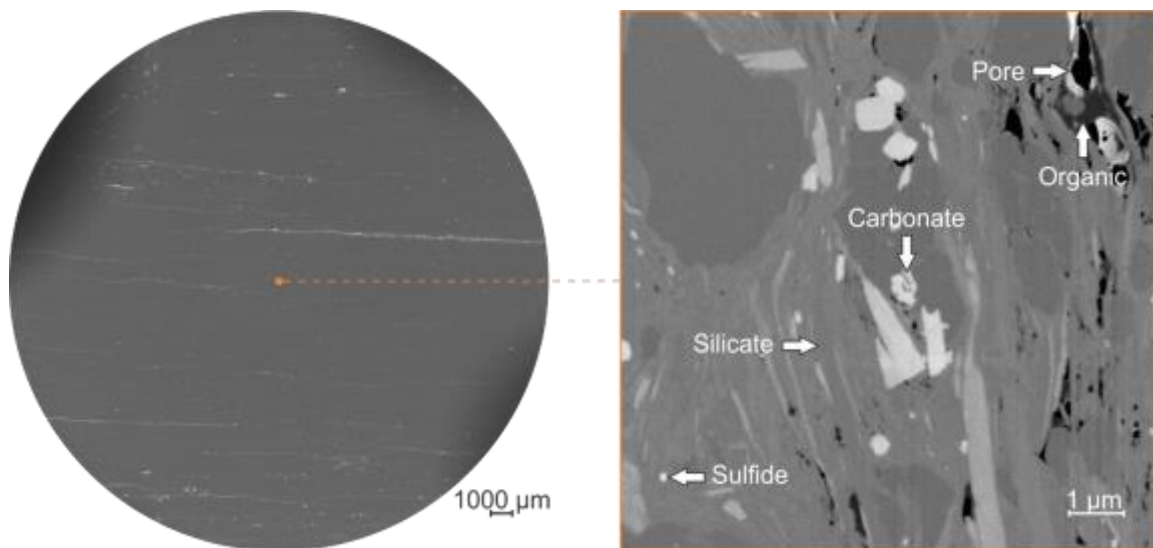


Figure 5.1. Scanning electron microscopy (SEM) image of the Woodford Shale.

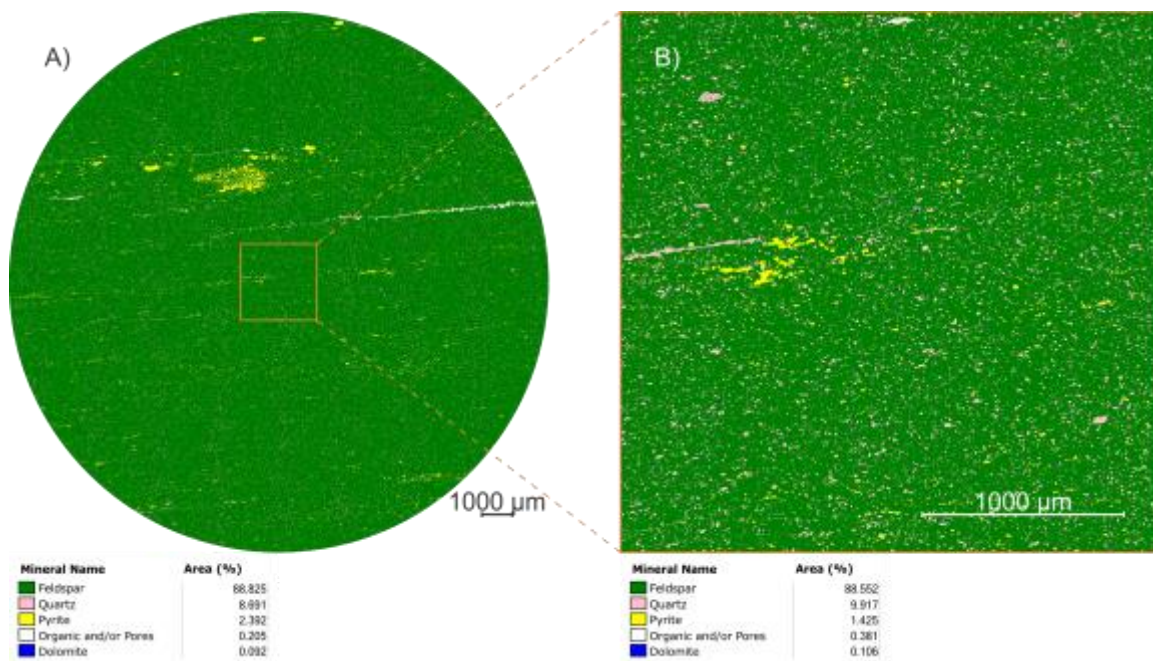


Figure 5.2. Automated mineralogy and petrography (A) 10 μm resolution and (B) 2 μm resolution mosaic image of the Woodford Shale.

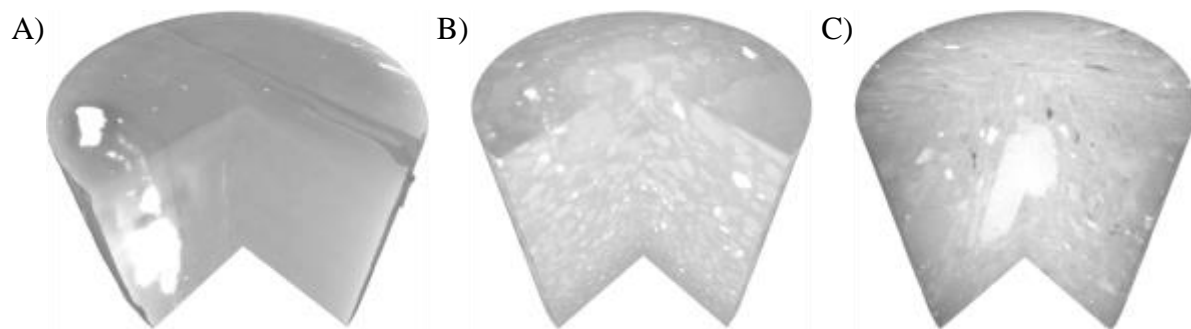


Figure 5.3. (A) 25-mm diameter micro-XRM (25 μm resolution), (B) 2.5-mm diameter micro-XRM (2.5 μm resolution), and (C) 65-μm diameter nano-XRM (150 nm resolution) models of the Woodford Shale.

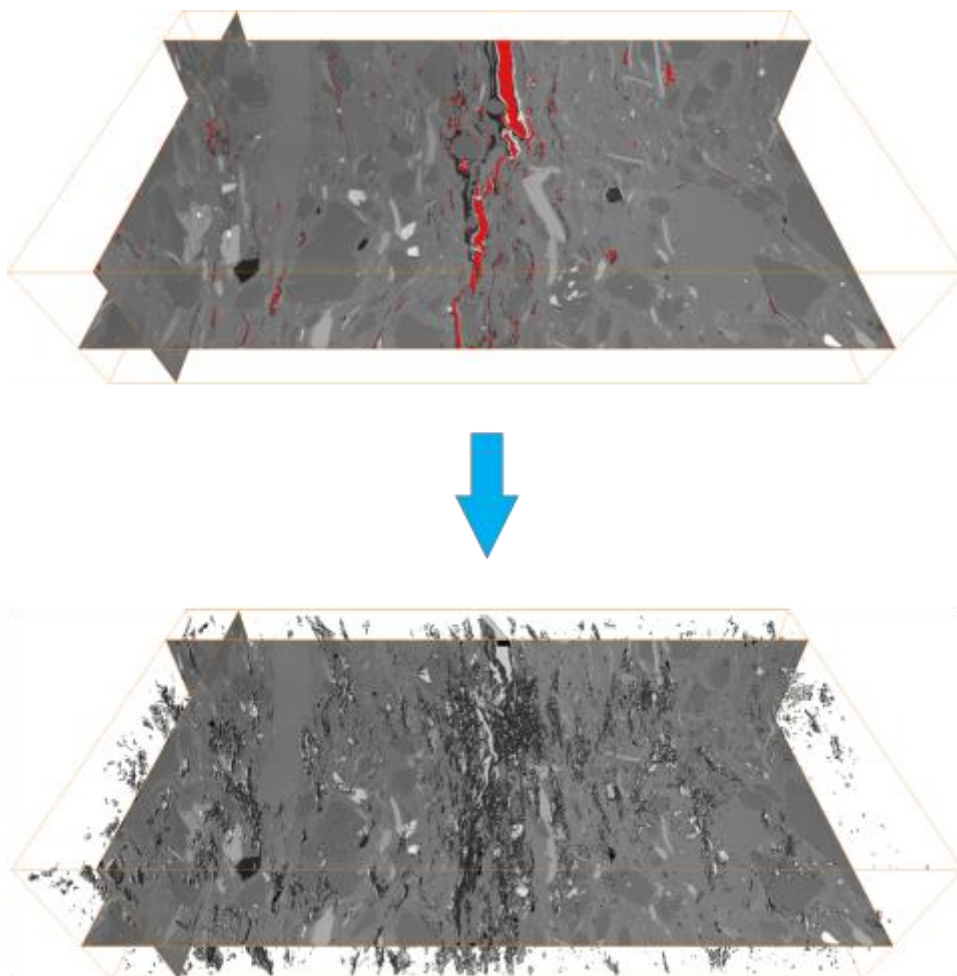


Figure 5.4. From image processing and segmentation, through model reconstruction and visualization, to pore network modeling workflow (red color indicates segmented pores and microfractures).

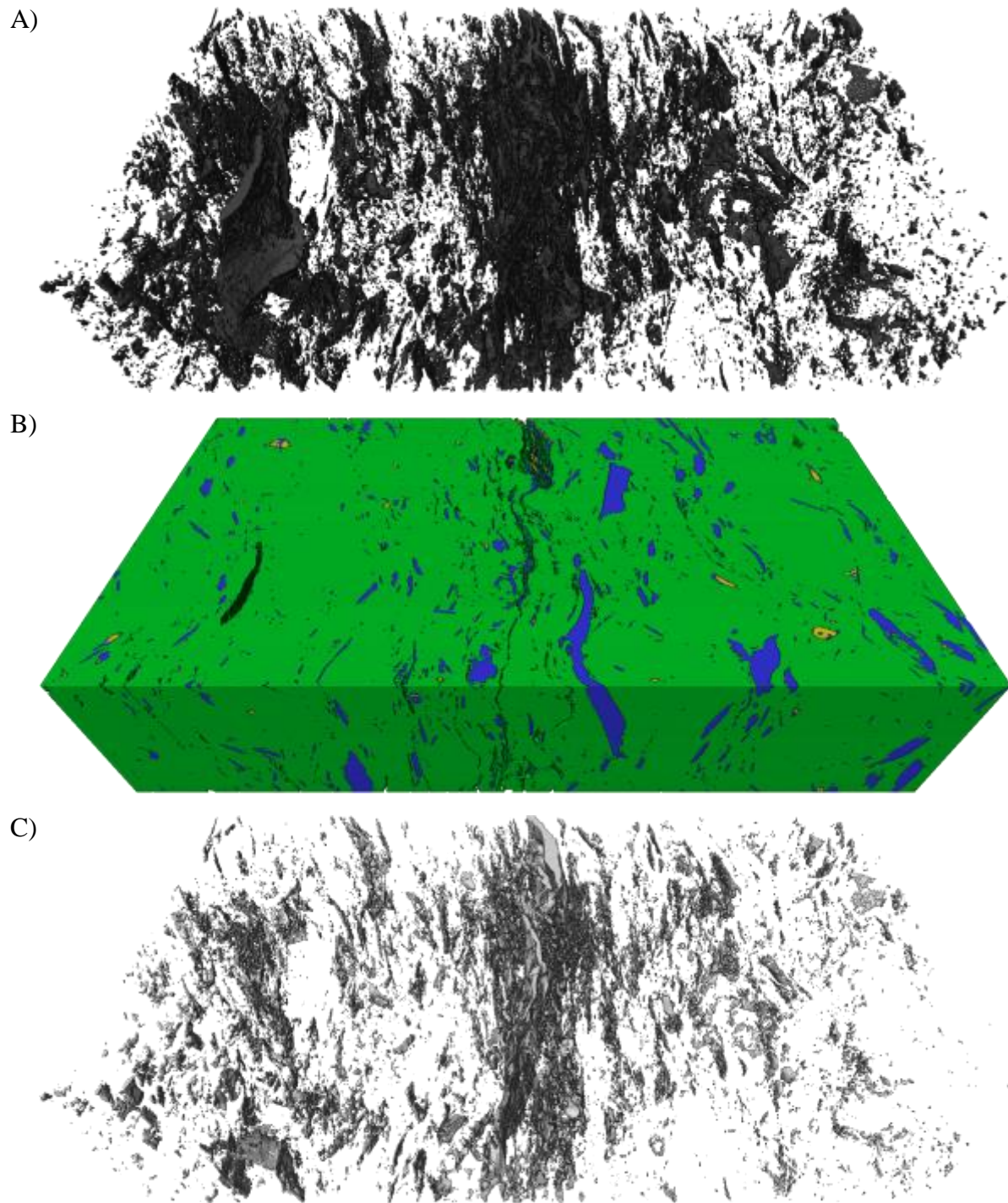


Figure 5.5. Focused ion beam scanning electron microscopy (FIB-SEM) model of (A) organic matter, (B) nonorganic matter, and (C) pore network (gray – total pores and microfractures, black – organic matter, green – silicate, blue – carbonate, yellow – sulfide) within the Woodford Shale.

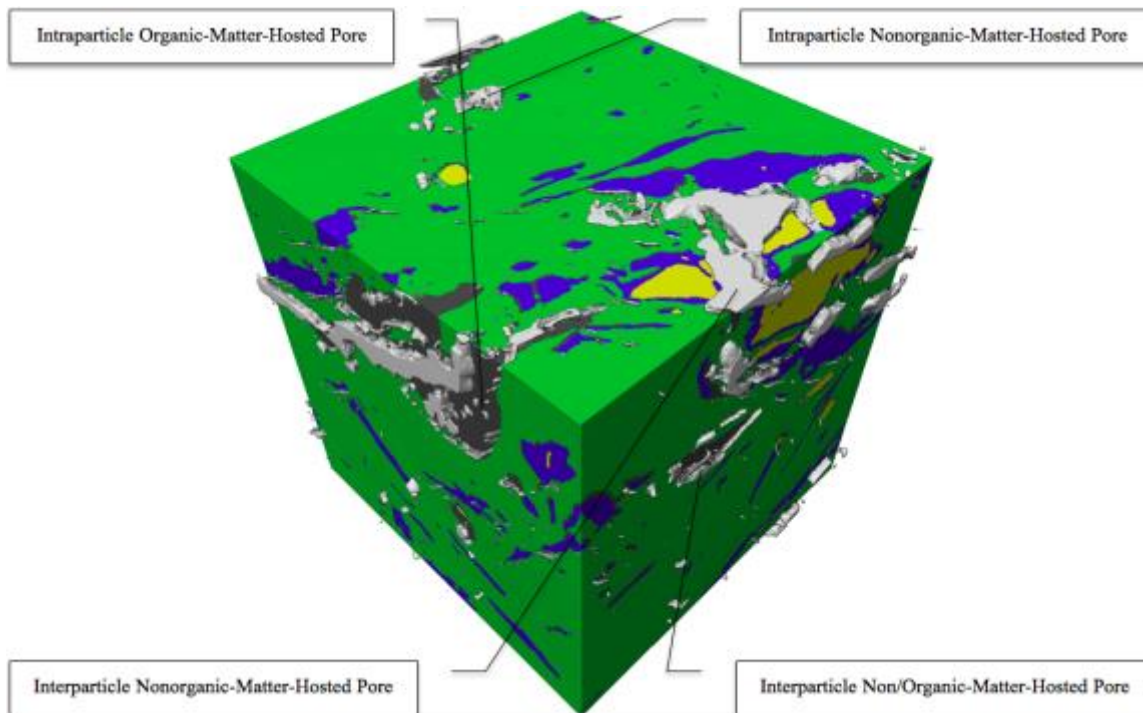


Figure 5.6. Pore types within $5 \mu\text{m}^3$ shale rock matrix: (a) intraparticle organic-matter-hosted pore located within single organic particle, (b) intraparticle nonorganic-matter-hosted pore located within single mineral particle, (c) interparticle nonorganic-matter-hosted pore located between mineral grains and crystals, and (d) interparticle non/organic-matter-hosted pore located at the interface of organic and mineral phases (gray – pores, black – organic matter, green – silicate, blue – carbonate, yellow – sulfide).

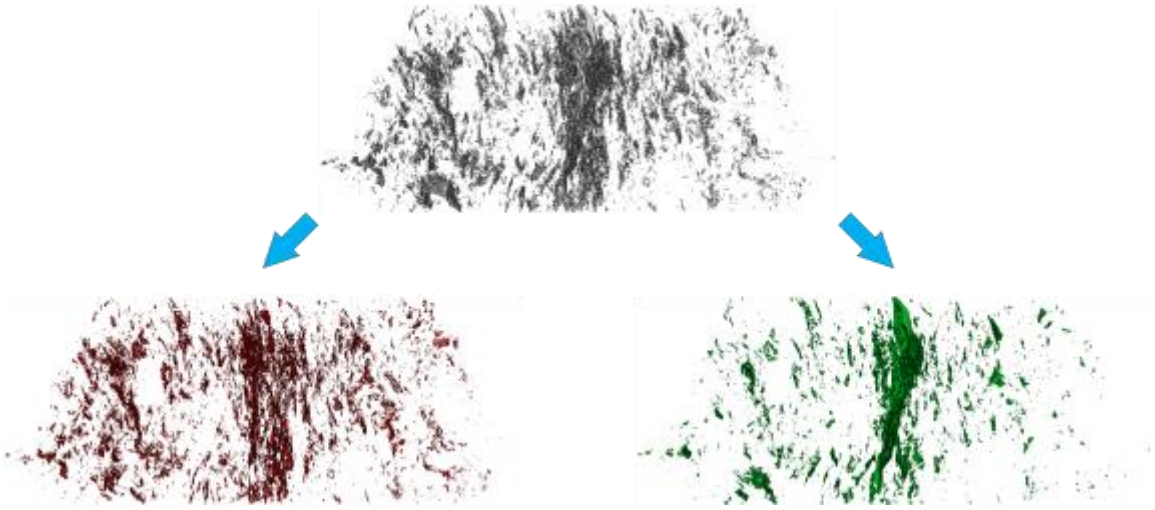


Figure 5.7. Pore network separation into organic-matter-hosted pores and nonorganic-matter-hosted pores (gray – total pore network, red – organic-matter-hosted pores, green – nonorganic-matter-hosted pores) within the Woodford Shale.

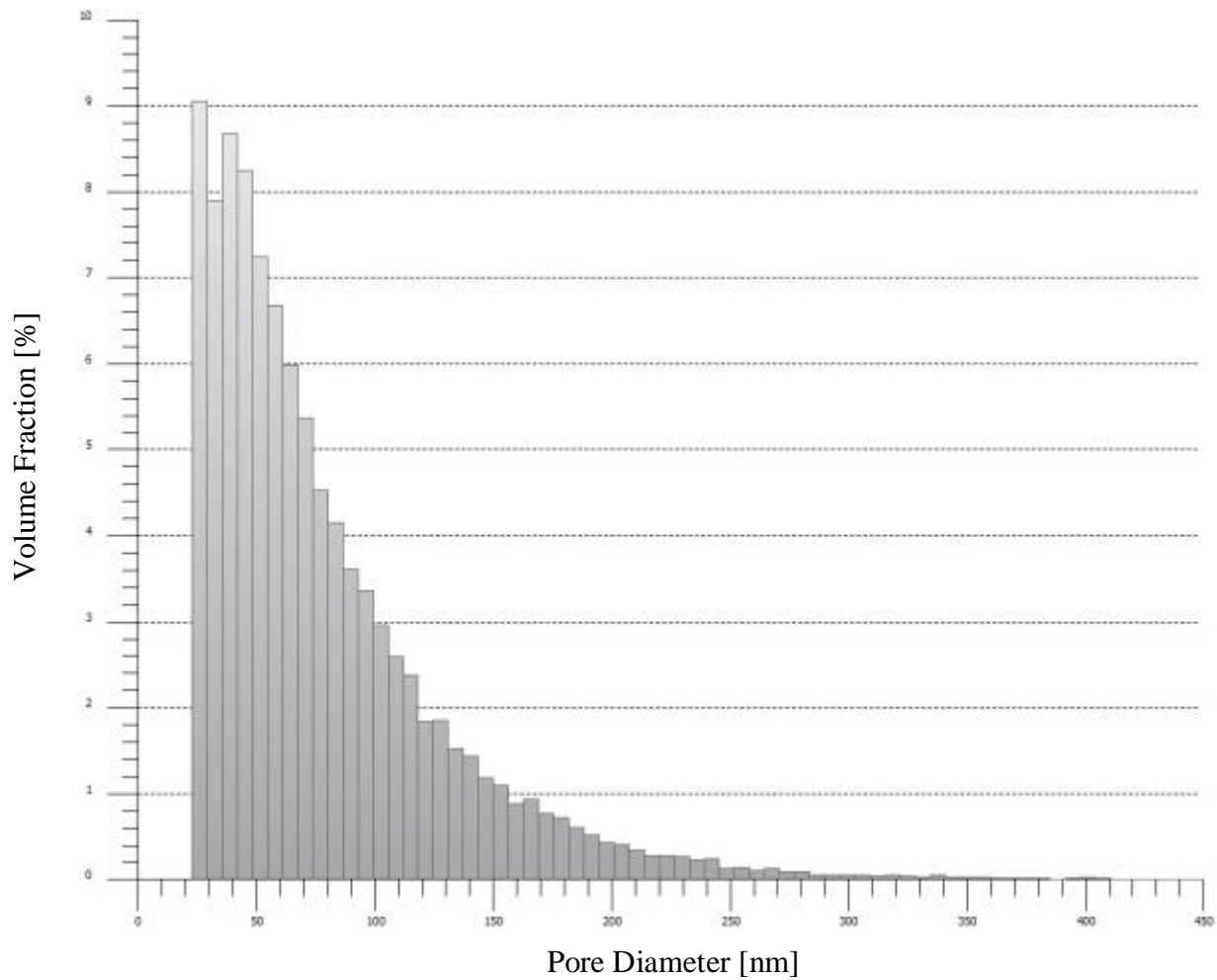


Figure 5.8. Pore size distribution of the organic-matter-hosted pores within the Woodford Shale.

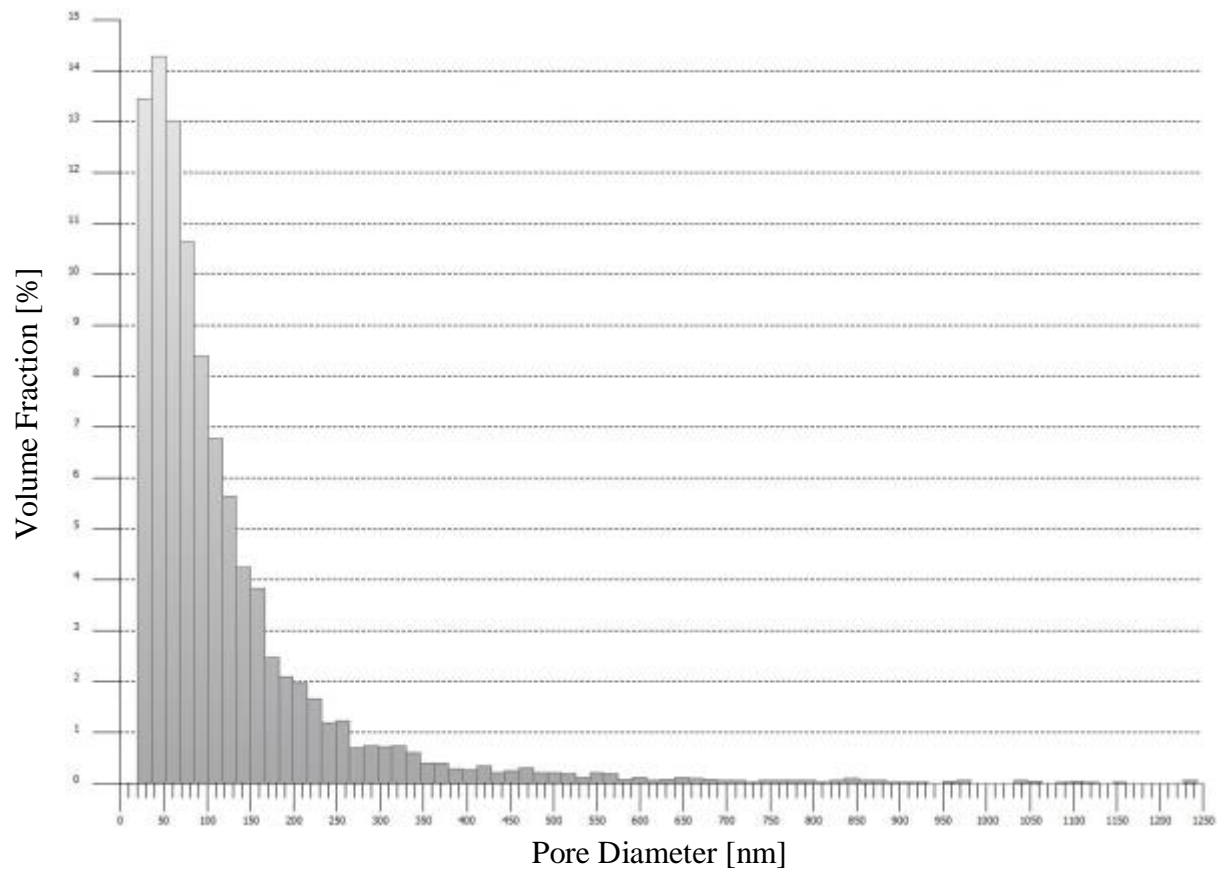


Figure 5.9. Pore size distribution of the nonorganic-matter-hosted pores within the Woodford Shale.

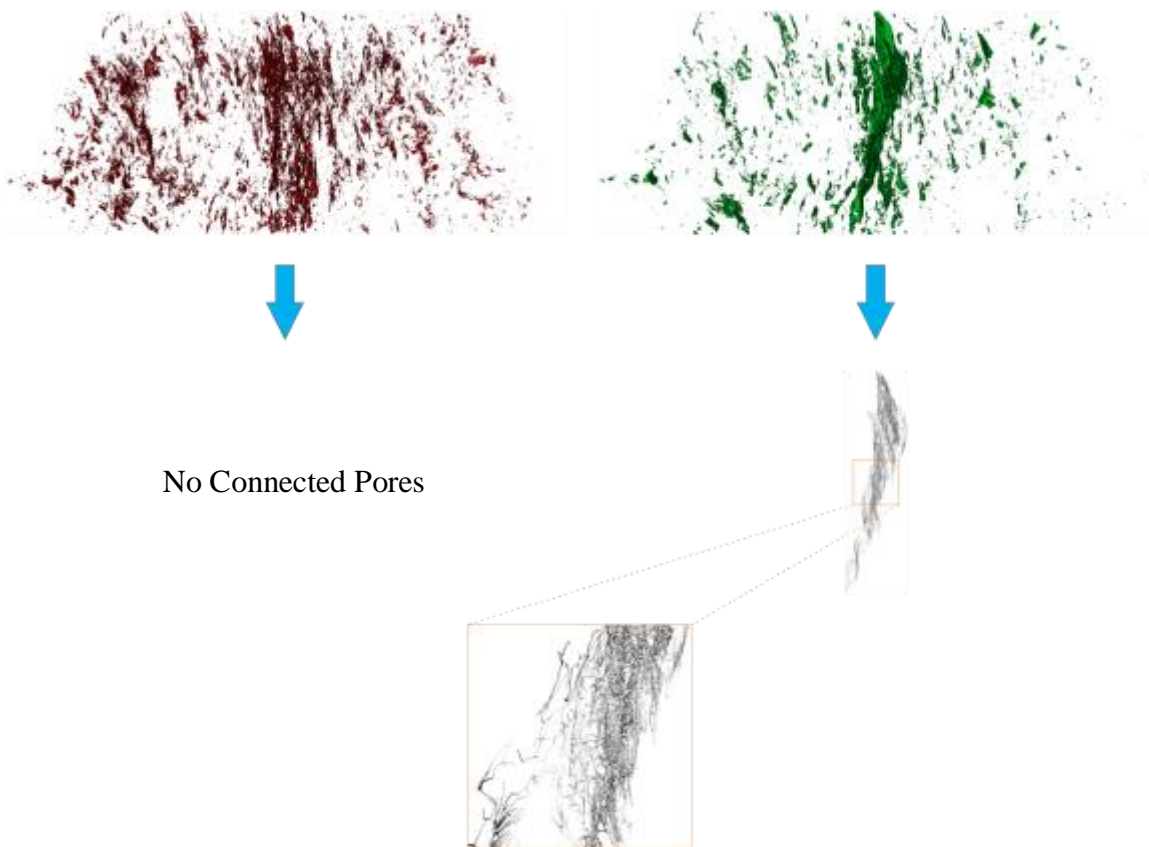


Figure 5.10. Connected pore network model of organic-matter-hosted and nonorganic-matter-hosted pores (red – organic-matter-hosted pores, green – nonorganic-matter-hosted pores) within the Woodford Shale.

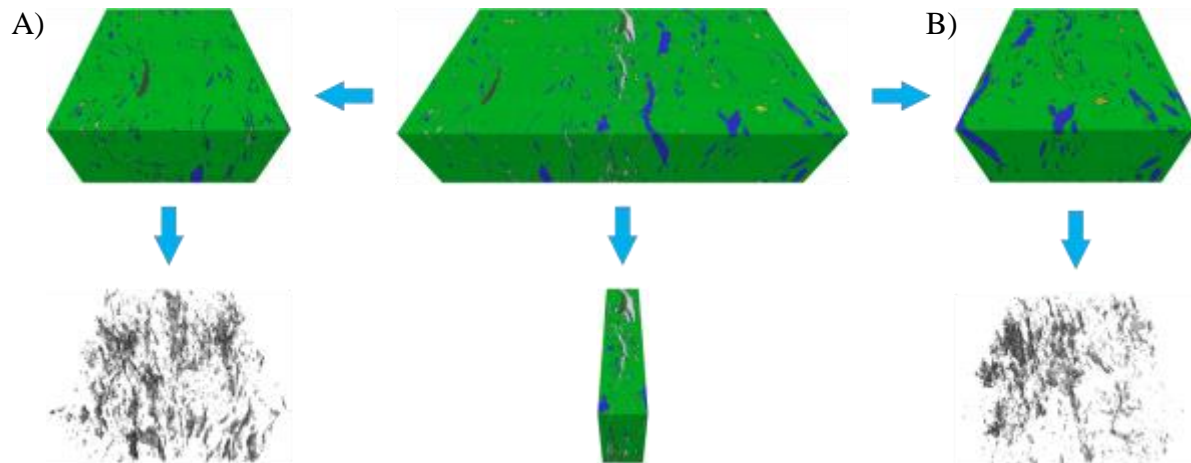


Figure 5.11. Focused ion beam scanning electron microscopy (FIB-SEM) model of the Woodford Shale divided into (A) region I and (B) region II (gray – pore network, black – organic matter, green – silicate, blue – carbonate, yellow – sulfide).

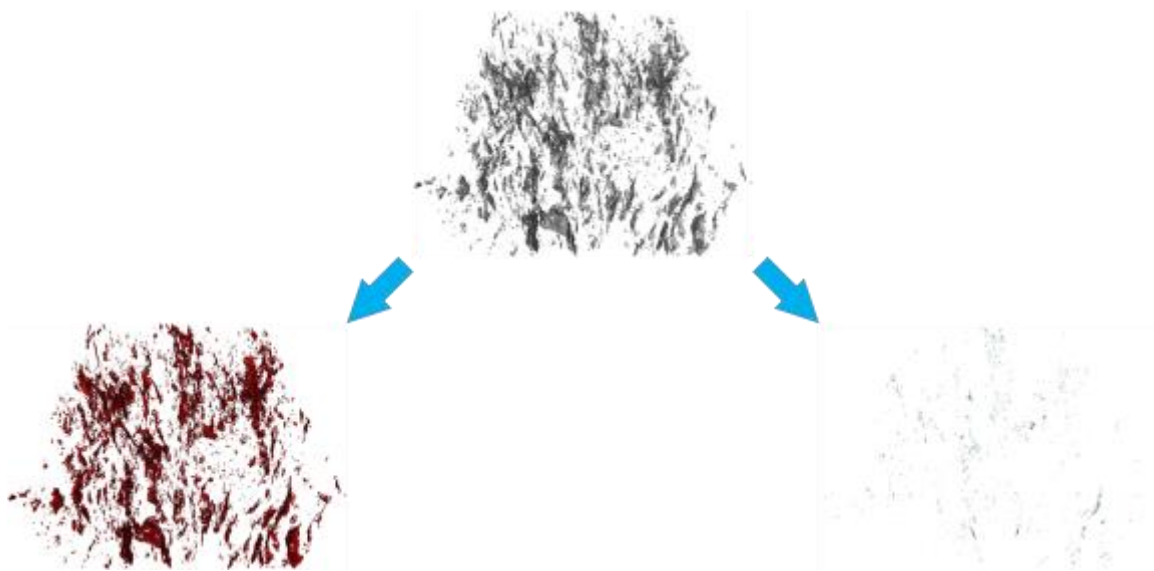


Figure 5.12. Pore network separation into organic-matter-related and nonorganic-matter-related pore network within the Woodford Shale in the region I (gray – total pore network, red – organic-matter-related pore network, green – nonorganic-matter-related pore network).

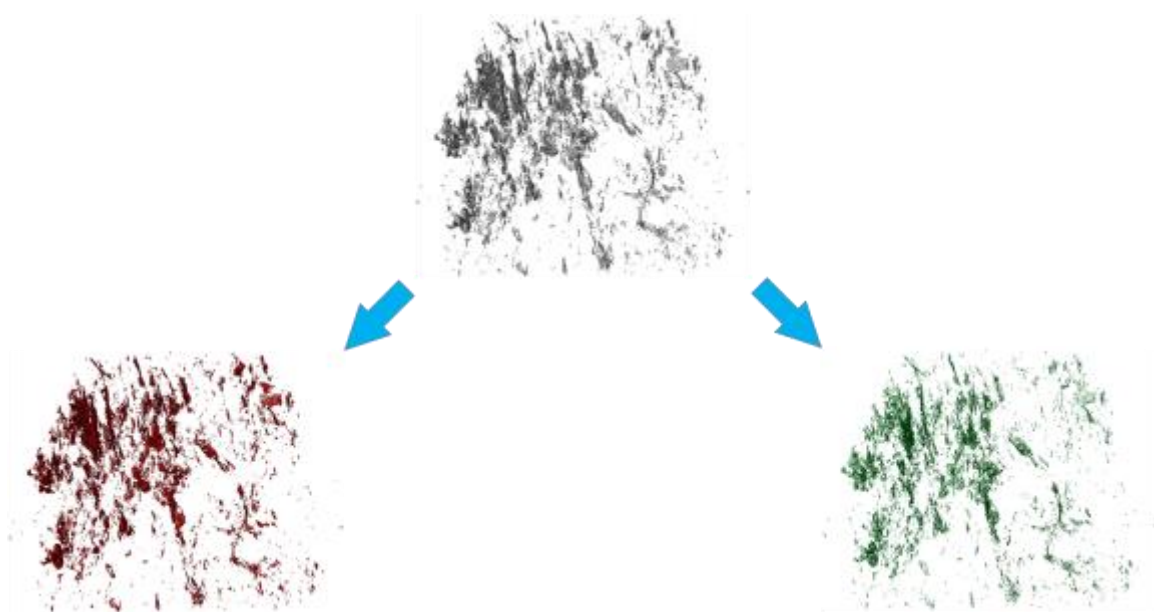


Figure 5.13. Pore network separation into organic-matter-related and nonorganic-matter-related pore network within the Woodford Shale in the region II (gray – total pore network, red – organic-matter-related pore network, green – nonorganic-matter-related pore network).

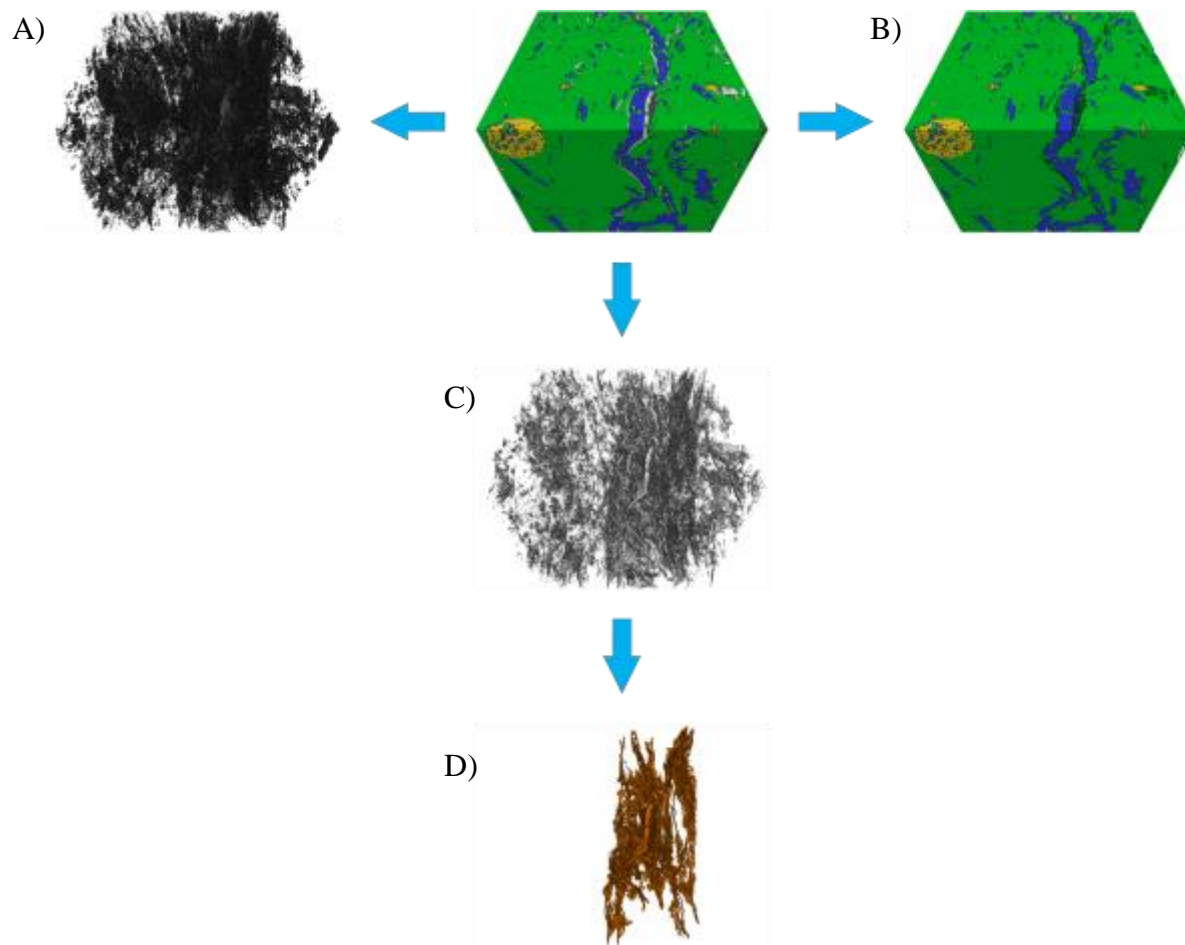


Figure 5.14. Focused ion beam scanning electron microscopy (FIB-SEM) model of (A) organic matter, (B) nonorganic matter, (C) total pore network, and (D) connected pore network (gray – total pores and microfractures, orange – connected pores and microfractures, black – organic matter, green – silicate, blue – carbonate, yellow – sulfide) within the Marcellus Shale.

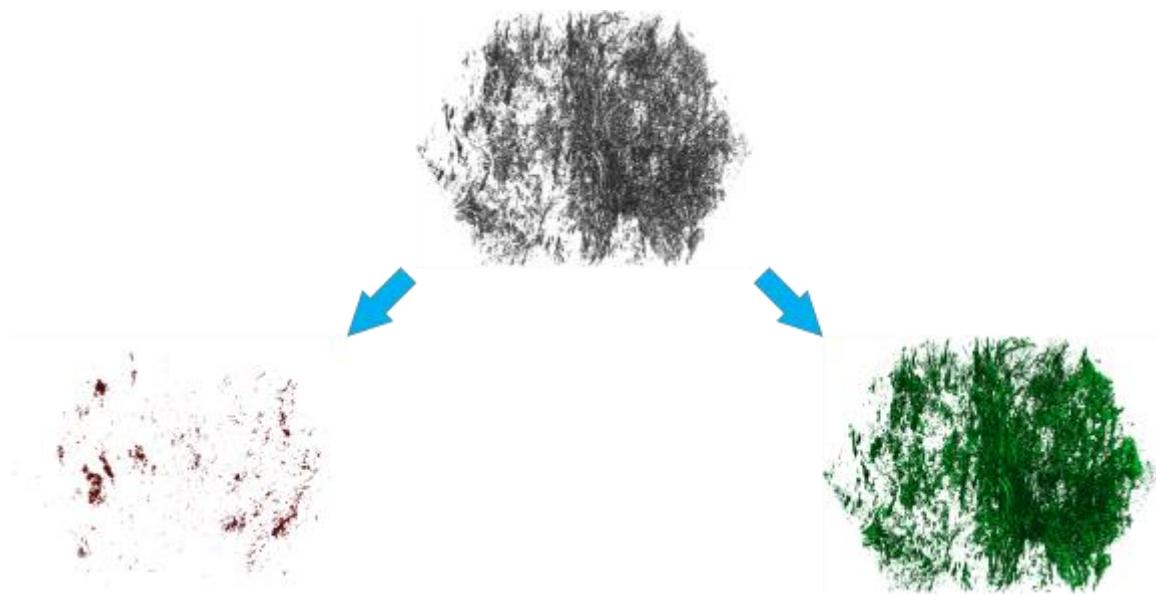


Figure 5.15. Pore network separation into organic-matter-hosted pores and nonorganic-matter-hosted pores (gray – total pore network, red – organic-matter-hosted pores, green – nonorganic-matter-hosted pores) within the Marcellus Shale.

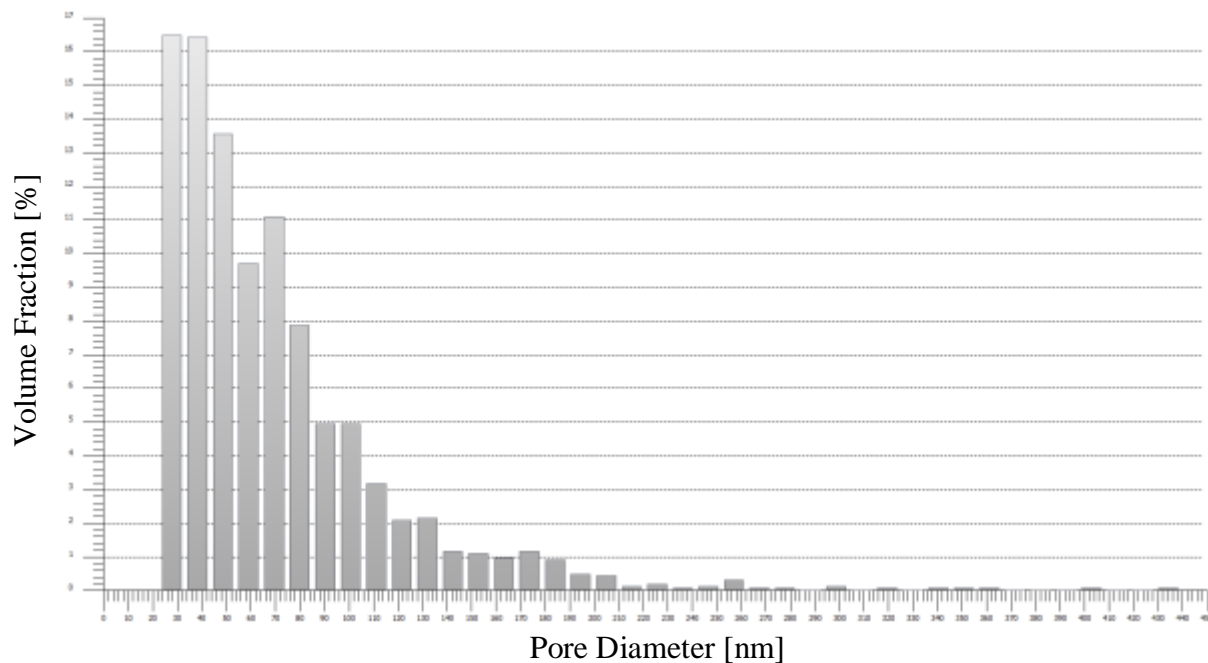


Figure 5.16. Pore size distribution of the organic-matter-hosted pores within the Marcellus Shale.

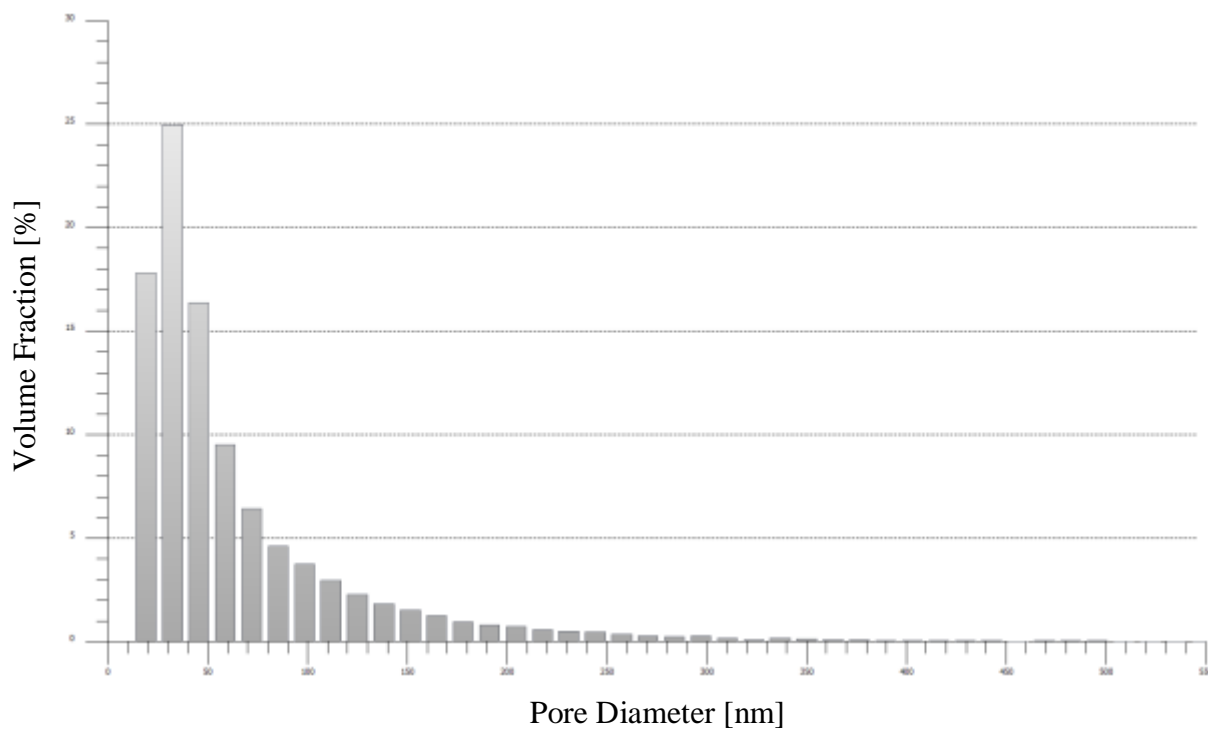


Figure 5.17. Pore size distribution of the nonorganic-matter-hosted pores within the Marcellus Shale.

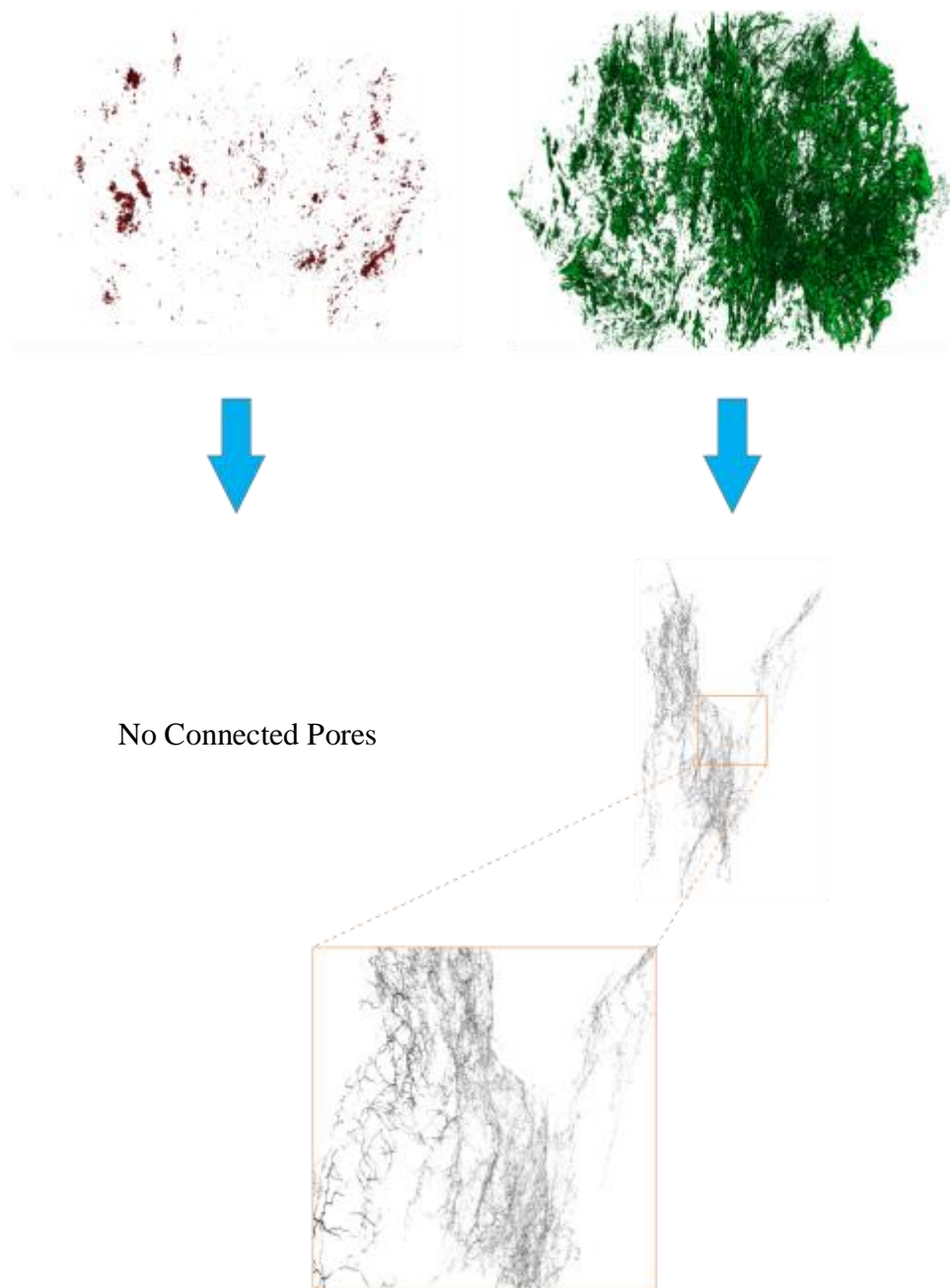


Figure 5.18. Connected pore network model of organic-matter-hosted and nonorganic-matter-hosted pores (red – organic-matter-hosted pores, green – nonorganic-matter-hosted pores) within the Marcellus Shale.

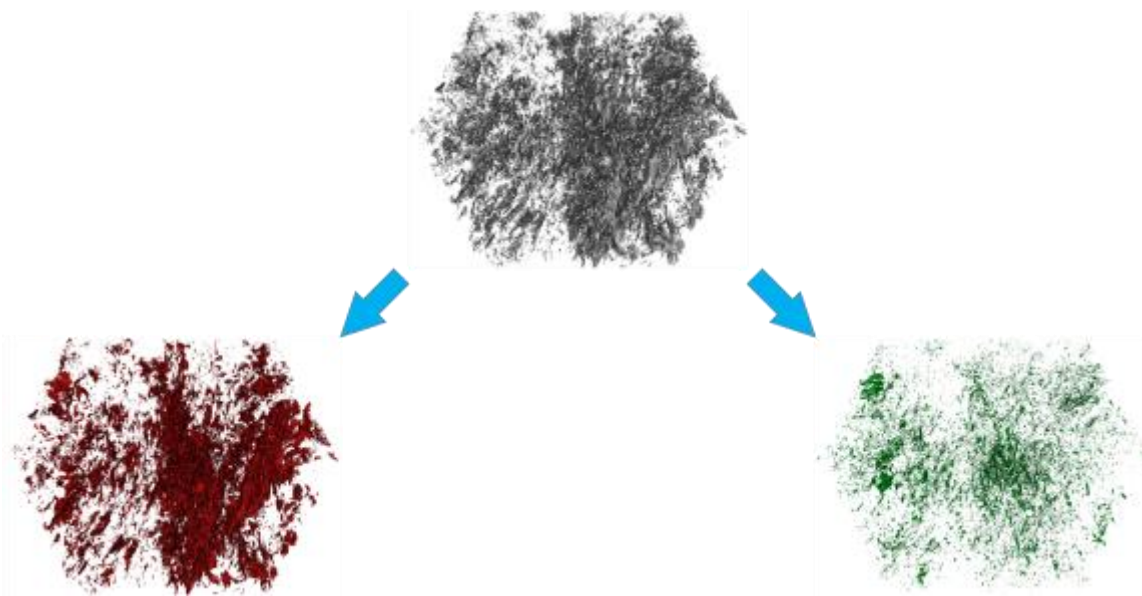


Figure 5.19. Pore network separation into organic-matter-related pores and nonorganic-matter-related pores (gray – total pore network, red – organic-matter-related pores, green – nonorganic-matter-related pores) within the Marcellus Shale.

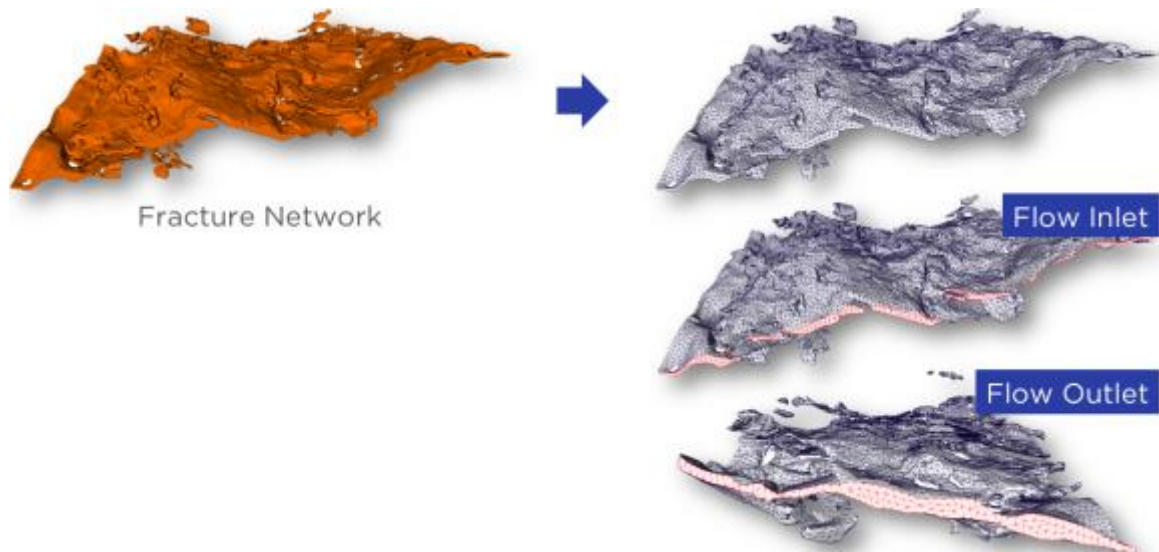


Figure 5.20. Tetrahedron volume mesh of the pore/fracture network.

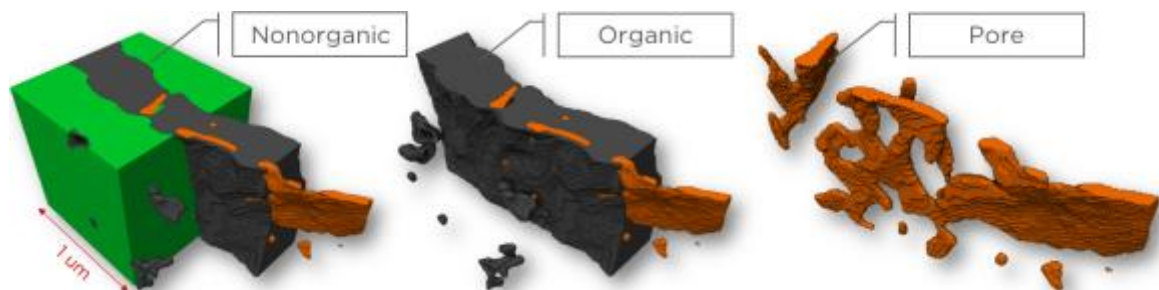


Figure 5.21. Three-phase (pore network, organic matter, and nonorganic matter) $1\ \mu\text{m} \times 1\ \mu\text{m} \times 2\ \mu\text{m}$ region of interest (ROI) of the FIB-SEM model of the Woodford Shale.

CHAPTER 6

CONCLUSIONS

In recent years, the development of shale reservoirs has attracted wide attention from the international energy industry. Increased interest in shale reservoir characterization has sparked development of novel approaches to reservoir analysis, incorporating many modern imaging instruments and powerful modeling, simulation, and visualization techniques. Because the success of unconventional oil and gas development is highly dependent on understanding the effect of matrix morphology and its properties on transport phenomena over multiple scales in the shale reservoirs, core measurements should occur at the front end of formation evaluation.

In this study, an investigation has been performed on heterogeneous shale rock matrix using samples from the Woodford Shale and the Marcellus Shale.

- Correlative micro-X-ray microscopy (micro-XRM), nano-X-ray microscopy (nano-XRM), and focused ion beam scanning electron microscopy (FIB-SEM) multiscale scientific digital imaging and digital rock physics workflow has been shown to be a powerful characterization technique for heterogeneous shale geomaterials. A comparison of the multiscale (micro-XRM, nano-XRM, and FIB-SEM) models suggests that no single method can fully capture the highly variable and complex nature of these rocks.

- In this study, there are two general approaches for pore network modeling presented. Both (non)organic-matter-hosted and (non)organic-matter-related pore systems were investigated. The PNM study has shown that both the Woodford Shale and the Marcellus Shale consist of intraparticle organic- and nonorganic-matter-hosted pores, interparticle nonorganic (mineral) pores, and pores located at the interface of organic and mineral phases (interparticle non/organic-matter-hosted pores). The results suggest that pores developed at the interface of organic and mineral phases strongly dominate over any other pore types within both the Woodford Shale and the Marcellus Shale FIB-SEM models. Interparticle non/organic-matter-hosted pore network has been demonstrated to have the potential for better connectivity than intraparticle organic- and nonorganic-matter-hosted pore systems. This study opens a door to more detailed study on three-dimensional heterogeneous shale reservoir pore systems, their connectivity, and their relationship with oil and gas production mechanisms. These problems will be addressed in future works.
- In this study, an image-to-simulation framework is also presented that provides a viable tool for finite element mesh generation of complex pore/fracture networks, identified using XRM and FIB-SEM, for any further modeling and simulation of continuum or non-continuum fluid flow in heterogeneous petroleum geomaterials.

REFERENCES

- Alharthy, N. S., Al Kobaisi, M., Kazemi, H., & Graves, R. M. (2012, January). Physics and modeling of gas flow in shale reservoirs. In *Abu Dhabi International Petroleum Conference and Exhibition*. Society of Petroleum Engineers.
- Alqahtani, A. A., & Tutuncu, A. N. (2014, August). Quantification of total organic carbon content in shale source rocks: An Eagle Ford case study. In *Unconventional Resources Technology Conference, Denver, Colorado, 25-27 August 2014* (pp. 382-398). Society of Exploration Geophysicists, American Association of Petroleum Geologists, Society of Petroleum Engineers.
- Amann-Hildenbrand, A., Ghanizadeh, A., & Krooss, B. M. (2012). Transport properties of unconventional gas systems. *Marine and Petroleum Geology*, *31*(1), 90-99.
- Ambrose, R. J., Hartman, R. C., Diaz Campos, M., Akkutlu, I. Y., & Sondergeld, C. (2010, January). New pore-scale considerations for shale gas in place calculations. In *SPE Unconventional Gas Conference*. Society of Petroleum Engineers.
- Ambrose, R. J., Hartman, R. C., Diaz-Campos, M., Akkutlu, I. Y., & Sondergeld, C. H. (2012). Shale gas-in-place calculations part I: New pore-scale considerations. *SPE Journal*, *17*(01), 219-229.
- Aplin, A. C., & Macquaker, J. H. (2011). Mudstone diversity: Origin and implications for source, seal, and reservoir properties in petroleum systems. *AAPG Bulletin*, *95*(12), 2031-2059.
- Bai, M. (2011, January). Improved understanding of stimulating tight shale gas reservoirs. In *SPE Production and Operations Symposium*. Society of Petroleum Engineers.
- Bin, B., Rukai, Z., Songtao, W., Wenjing, Y. A. N. G., Gelb, J., Gu, A., ... & Ling, S. U. (2013). Multi-scale method of Nano (Micro)-CT study on microscopic pore structure of tight sandstone of Yanchang Formation, Ordos Basin. *Petroleum Exploration and Development*, *40*(3), 354-358.
- Bertoncello, A., & Honarpour, M. M. (2013, September). Standards for characterization of rock properties in unconventional reservoirs: Fluid flow mechanism, quality control, and uncertainties. In *SPE Annual Technical Conference and Exhibition*. Society of Petroleum Engineers.

Blunt, M. J., Bijeljic, B., Dong, H., Gharbi, O., Iglauer, S., Mostaghimi, P., ... & Pentland, C. (2013). Pore-scale imaging and modelling. *Advances in Water Resources*, 51, 197-216.

Bruner, K. R. (2011). A comparative study of the Mississippian Barnett shale, Fort Worth basin, and Devonian Marcellus shale, Appalachian basin. *DOE/NETL-2011/1478*

Bustin, R. M., Bustin, A. M., Cui, A., Ross, D., & Pathi, V. M. (2008, January). Impact of shale properties on pore structure and storage characteristics. In *SPE Shale Gas Production Conference*. Society of Petroleum Engineers.

Cardott, B. J. (2012). Thermal maturity of Woodford Shale gas and oil plays, Oklahoma, USA. *International Journal of Coal Geology*, 103, 109-119.

Chalmers, G. R., Bustin, R. M., & Power, I. M. (2012). Characterization of gas shale pore systems by porosimetry, pycnometry, surface area, and field emission scanning electron microscopy/transmission electron microscopy image analyses: Examples from the Barnett, Woodford, Haynesville, Marcellus, and Doig units. *AAPG Bulletin*, 96(6), 1099-1119.

Chen, C., Hu, D., Westacott, D., & Loveless, D. (2013). Nanometer-scale characterization of microscopic pores in shale kerogen by image analysis and pore-scale modeling. *Geochemistry, Geophysics, Geosystems*, 14(10), 4066-4075.

Chen, R., Sharma, S., Bank, T., Soeder, D., & Eastman, H. (2015). Comparison of isotopic and geochemical characteristics of sediments from a gas-and liquids-prone wells in Marcellus shale from Appalachian Basin, West Virginia. *Applied Geochemistry*, 60, 59-71.

Collell, J., Galliero, G., Vermorel, R., Ungerer, P., Yiannourakou, M., Montel, F., & Pujol, M. (2015). Transport of multicomponent hydrocarbon mixtures in shale organic matter by molecular simulations. *The Journal of Physical Chemistry C*, 119(39), 22587-22595.

Curtis, M. E., Ambrose, R. J., & Sondergeld, C. H. (2010, January). Structural characterization of gas shales on the micro-and nano-scales. In *Canadian Unconventional Resources and International Petroleum Conference*. Society of Petroleum Engineers.

Curtis, M. E., Ambrose, R. J., Sondergeld, C. H., & Rai, C. S. (2011, January). Investigation of the relationship between organic porosity and thermal maturity in the Marcellus Shale. In *North American Unconventional Gas Conference and Exhibition*. Society of Petroleum Engineers.

Curtis, M. E., Sondergeld, C. H., Ambrose, R. J., & Rai, C. S. (2012). Microstructural investigation of gas shales in two and three dimensions using nanometer-scale resolution imaging. *AAPG Bulletin*, 96(4), 665-677.

Curtis, M. (2014). Mapping of organic matter distribution in shales on the centimeter scale with nanometer resolution. *Unconventional Resources Technology Conference (URTEC)*.

Darabi, H., Ettehad, A., Javadpour, F., & Sepehrnoori, K. (2012). Gas flow in ultra-tight shale strata. *Journal of Fluid Mechanics*, 710, 641.

Dewers, T. A., Heath, J., Ewy, R., & Duranti, L. (2012). Three-dimensional pore networks and transport properties of a shale gas formation determined from focused ion beam serial imaging. *International Journal of Oil, Gas and Coal Technology*, 5(2-3), 229-248.

Ding, W., Li, C., Li, C., Xu, C., Jiu, K., Zeng, W., & Wu, L. (2012). Fracture development in shale and its relationship to gas accumulation. *Geoscience Frontiers*, 3(1), 97-105.

Fogden, A., McKay, T., Turner, M., Marathe, R., & Senden, T. (2014, August). Micro-CT analysis of pores and organics in unconventional using novel contrast strategies. In *Unconventional Resources Technology Conference, Denver, Colorado, 25-27 August 2014* (pp. 960-969). Society of Exploration Geophysicists, American Association of Petroleum Geologists, Society of Petroleum Engineers.

Geiger, S., Schmid, K. S., & Zaretskiy, Y. (2012). Mathematical analysis and numerical simulation of multi-phase multi-component flow in heterogeneous porous media. *Current Opinion in Colloid & Interface Science*, 17(3), 147-155.

Gelb, J., Gu, A., Fong, T., Hunter, L., Lau, S. H., & Yun, W. (2011, September). A closer look at shale: Representative elementary volume analysis with laboratory 3D X-Ray computed microtomography and nanotomography. *International Symposium of the Society of Core Analysts*.

Gelb, J., Roth, S., Dong, H., Li, D., Gu, A., Yun, S., & Yun, W. (2012). Non-destructive local X-ray tomography for multi-length scale analysis of reservoir rocks: Validations and observations. *International Symposium of the Society of Core Analysts*.

Goldstein, J.I., Newbury, D.E., Echlin, P., Joy, D.C., Fiori, C., & Lifshin, E. (1981). *Scanning electron microscopy and X-ray microanalysis. A text for biologists, materials scientists, and geologists*. Plenum Publishing Corporation.

Goral, J., & Miskovic, I. (2015). A workflow for multi-scale modeling and simulation of transport phenomena in Woodford Shale rock matrix. *Unconventional Resources Technology Conference (URTEC)*.

Goral, J., Miskovic, I., Gelb, J., & Kasahara, J. (2015a, November). Pore network investigation in Marcellus Shale rock matrix. In *SPE Asia Pacific Unconventional Resources Conference and Exhibition*. Society of Petroleum Engineers.

Goral, J., Miskovic, I., Gelb, J., & Andrew, M. (2015b, December). Correlative XRM and FIB-SEM for non/organic pore network modeling in Woodford Shale rock matrix. In *International Petroleum Technology Conference*. International Petroleum Technology Conference.

Goral, J., Miskovic, I., Gelb, J., & Marsh, M. (2016). Correlative X-ray and electron microscopy for multi-scale characterization of heterogeneous shale reservoir pore systems. *AAPG Memoir*, 112, 77–88.

Guan, Y., Li, W., Gong, Y., Liu, G., Zhang, X., Chen, J., ... & Wang, H. (2011). Analysis of the three-dimensional microstructure of a solid-oxide fuel cell anode using nano X-ray tomography. *Journal of Power Sources*, 196(4), 1915-1919.

Heath, J. E., Dewers, T. A., McPherson, B. J., Petrusak, R., Chidsey, T. C., Rinehart, A. J., & Mozley, P. S. (2011). Pore networks in continental and marine mudstones: Characteristics and controls on sealing behavior. *Geosphere*, 7(2), 429-454.

Herman, G. T. (2009). *Fundamentals of computerized tomography: Image reconstruction from projections*. Springer Science & Business Media.

Hooghan, K. N. (2014). Protocol for finalizing locations for FIB/SEM cubes on shale samples: General guidelines with up scaling in mind. *Unconventional Resources Technology Conference (URTEC)*.

Huang, J., Cavanaugh, T., & Nur, B. (2013). 1 An introduction to SEM operational principles and geologic applications for shale hydrocarbon reservoirs. *AAPG Memoir*, 102, 1–6.

Hyne, N. J. (2012). *Nontechnical guide to petroleum geology, exploration, drilling, and production*. PennWell Books.

Javadpour, F., Fisher, D., & Unsworth, M. (2007). Nanoscale gas flow in shale gas sediments. *Journal of Canadian Petroleum Technology*, 46(10).

King, G. E. (2012, January). Hydraulic fracturing 101: What every representative, environmentalist, regulator, reporter, investor, university researcher, neighbor and engineer should know about estimating frac risk and improving frac performance in unconventional gas and oil wells. In *SPE Hydraulic Fracturing Technology Conference*. Society of Petroleum Engineers.

Knackstedt, M., Golab, A., & Riepe, L. (2012, June). Petrophysical characterization of unconventional reservoir core at multiple scales. In *SPWLA 53rd Annual Logging Symposium*. Society of Petrophysicists and Well-Log Analysts.

Lemmens, H. J., Butcher, A. R., & Botha, P. W. S. K. (2011). FIB/SEM and SEM/EDX: A new dawn for the SEM in the core lab?. *Petrophysics*, 52(06), 452-456.

Lønøy, A. (2006). Making sense of carbonate pore systems. *AAPG Bulletin*, 90(9), 1381-1405.

Lopez, O., Mock, A., Øren, P. E., Long, H., Kalam, Z., Vahrenkamp, V., ... & Al Hosni, H. (2012, August). Validation of fundamental carbonate reservoir core properties using digital rock physics. In *International Symposium of the Society of Core Analysts, SCA2012-19*.

Loucks, R. G., Reed, R. M., Ruppel, S. C., & Jarvie, D. M. (2009). Morphology, genesis, and distribution of nanometer-scale pores in siliceous mudstones of the Mississippian Barnett Shale. *Journal of Sedimentary Research*, 79(12), 848-861.

Loucks, R. G., Reed, R. M., Ruppel, S. C., & Hammes, U. (2010). Preliminary classification of matrix pores in mudrocks. *Gulf Coast Association of Geological Societies Transactions*, 60, 435-441.

Loucks, R. G., Reed, R. M., Ruppel, S. C., & Hammes, U. (2012). Spectrum of pore types and networks in mudrocks and a descriptive classification for matrix-related mudrock pores. *AAPG Bulletin*, 96(6), 1071-1098.

Lu, J., Ruppel, S. C., & Rowe, H. D. (2015). Organic matter pores and oil generation in the Tuscaloosa marine shale. *AAPG Bulletin*, 99(2), 333-357.

Ma, Y. Z., & Holditch, S. (2015). *Unconventional oil and gas resources handbook: Evaluation and development*. Gulf Professional Publishing.

Merkle, A. P., & Gelb, J. (2013). The ascent of 3D X-ray microscopy in the laboratory. *Microscopy Today*, 21(02), 10-15.

Merkle, A. P., Gelb, J., Orchowski, A., & Fuchs, J. (2014). X-ray microscopy: The cornerstone for correlative characterization methods in materials research and life science. *Microscopy and Microanalysis*, 20(S3), 986-987.

Milliken, K. L., Rudnicki, M., Awwiller, D. N., & Zhang, T. (2013). Organic matter-hosted pore system, Marcellus formation (Devonian), Pennsylvania. *AAPG Bulletin*, 97(2), 177-200.

Nadimi, S. (2015). *State-based peridynamics simulation of hydraulic fracture phenomenon in geological media* (The University of Utah).

Nadimi, S., Miscovic, I., & McLennan, J. (2016). A 3D peridynamic simulation of hydraulic fracture process in a heterogeneous medium. *Journal of Petroleum Science and Engineering*, 145, 444-452.

Nelson, P. H. (2009). Pore-throat sizes in sandstones, tight sandstones, and shales. *AAPG Bulletin*, 93(3), 329-340.

Passey, Q. R., Bohacs, K., Esch, W. L., Klimentidis, R., & Sinha, S. (2010, January). From oil-prone source rock to gas-producing shale reservoir-geologic and petrophysical characterization of unconventional shale gas reservoirs. In *International oil and gas conference and exhibition in China*. Society of Petroleum Engineers.

Pathak, M., Deo, M. D., Panja, P., & Levey, R. A. (2015, October). The effect of kerogen-hydrocarbons interaction on the pvt properties in liquid rich shale plays. In *SPE/CSUR Unconventional Resources Conference*. Society of Petroleum Engineers.

Pathak, M., Pawar, G., Huang, H., & Deo, M. D. (2015, November). Carbon dioxide sequestration and hydrocarbons recovery in the gas rich shales: An insight from the molecular dynamics simulations. In *Carbon Management Technology Conference*. Carbon Management Technology Conference.

Pathak, M., Panja, P., Levey, R., & Deo, M. (2017). Effect of the presence of organic matter on bubble points of oils in shales. *AIChE Journal*, 63, 3083-3095.

Pathak, M., Cho, H., & Deo, M. (2017). Experimental and molecular modeling study of bubble points of hydrocarbon mixtures in nanoporous media. *Energy & Fuels*, 31(4), 3427-3435.

Pommer, M., & Milliken, K. (2015). Pore types and pore-size distributions across thermal maturity, Eagle Ford Formation, southern Texas. *AAPG Bulletin*, 99(9), 1713-1744.

Saraji, S. (2014). High-resolution three-dimensional characterization of pore networks in shale reservoir rocks. *Unconventional Resources Technology Conference (URTEC)*.

Schlüter, S., Sheppard, A., Brown, K., & Wildenschild, D. (2014). Image processing of multiphase images obtained via X-ray microtomography: A review. *Water Resources Research*, 50(4), 3615-3639.

Shearing, P. R., Golbert, J., Chater, R. J., & Brandon, N. P. (2009). 3D reconstruction of SOFC anodes using a focused ion beam lift-out technique. *Chemical Engineering Science*, 64(17), 3928-3933.

Shi, J., Zhang, L., Li, Y., Yu, W., He, X., Liu, N., ... & Wang, T. (2013, November). Diffusion and flow mechanisms of shale gas through matrix pores and gas production forecasting. In *SPE Unconventional Resources Conference Canada*. Society of Petroleum Engineers.

Solano, N. A., Krause, F. F., & Clarkson, C. R. (2014, August). Characterization of cm-scale heterogeneities in a tight oil reservoir using X-ray computed tomography, profile permeability measurements and 3-D image analysis. In *Unconventional Resources Technology Conference, Denver, Colorado, 25-27 August 2014* (pp. 1057- 1062). Society of Exploration Geophysicists, American Association of Petroleum Geologists, Society of Petroleum Engineers.

Silin, D. B., & Kneafsey, T. J. (2011, January). Gas shale: From nanometer-scale observations to well modeling. In *Canadian Unconventional Resources Conference*. Society of Petroleum Engineers.

Takhar, P. S., & Zhang, S. (2009). Drying of corn kernels: From experimental images to multiscale multiphysics modeling. In *Proc. of the COMSOL Conf., Boston*.

Tkachuk, A., Duewer, F., Cui, H., Feser, M., Wang, S., & Yun, W. (2007). X-ray computed tomography in Zernike phase contrast mode at 8 keV with 50-nm resolution using Cu rotating anode X-ray source. *Zeitschrift für Kristallographie-Crystalline Materials*, 222(11/2007), 650-655.

Tono, H. (2008). Computing properties from 3-D imaging. *Hart's E & P*, 81(11), 100-101.

Outlook, A. E. (2010). Energy information administration. *Department of Energy*, 92010(9), 1-15.

Vega, B., Andrews, J. C., Liu, Y., Gelb, J., & Kovsky, A. (2013, August). Nanoscale visualization of gas shale pore and textural features. In *Unconventional resources technology conference* (pp. 1603-1613). Society of Exploration Geophysicists, American Association of Petroleum Geologists, Society of Petroleum Engineers.

Wang, C., Chen, Z., Yao, J., Sun, H., Yang, Y., & Wu, K. (2014, August). Organic and inorganic pore structure analysis in shale matrix with superposition method. In *Unconventional Resources Technology Conference, Denver, Colorado, 25-27 August 2014* (pp. 1079-1084). Society of Exploration Geophysicists, American Association of Petroleum Geologists, Society of Petroleum Engineers.

Waters, G. A., Lewis, R. E., & Bentley, D. (2011, January). The effect of mechanical properties anisotropy in the generation of hydraulic fractures in organic shales. In *SPE Annual Technical Conference and Exhibition*. Society of Petroleum Engineers.

Weng, X., Cohen, C. E., & Kresse, O. (2015). Impact of preexisting natural fractures on hydraulic fracture simulation. In Y.Z. Ma and S. A. Holditch, eds., *Unconventional Oil and Gas Resources Handbook: Evaluation and Development*, 289.

Xia, Y., Goral, J., Huang, H., Miskovic, I., Meakin, P., & Deo, M. (2017). Many-body dissipative particle dynamics modeling of fluid flow in fine-grained nanoporous shales. *Physics of Fluids*, 29(5), 056601.

Zagorski, W. A., Wrightstone, G. R., & Bowman, D. C. (2012). The Appalachian Basin Marcellus gas play: Its history of development, geologic controls on production, and future potential as a world-class reservoir, in J. A. Breyer, ed., *Shale reservoirs—Giant resources for the 21st century*. *AAPG Memoir*, 97, 172–200.

Zhai, Z., Wang, X., Jin, X., Sun, L., Li, J., & Cao, D. (2014). Adsorption and diffusion of shale gas reservoirs in modeled clay minerals at different geological depths. *Energy & Fuels*, 28(12), 7467-7473.

Zhang, S., Maestra, F. D., Combaret, N., Klimentidis, R., Barthelemy, P., Albou, R., & Bernard, D. (2011, March). The analysis and simulation of rock properties using FIBSEM and Virtual Material Studio. In *NAFEMS World Congress 2011* (pp. 22-26).